

SVEMnet: An R package for Self-Validated Elastic-Net Ensembles and Multi-Response Optimization in Small-Sample Mixture–Process Experiments

Andrew T. Karl^a

^a*Karl Statistical Services, Aurora, CO, 80016, USA*

Abstract

SVEMnet is an R package for fitting Self-Validated Ensemble Models (SVEM) with elastic-net base learners and performing multi-response optimization in small-sample mixture–process design-of-experiments (DOE) studies with numeric, categorical, and mixture factors. SVEMnet wraps elastic-net and relaxed elastic-net models for Gaussian and binomial responses from `glmnet` in a fractional random-weight (FRW) resampling scheme with anti-correlated train/validation weights; penalties are selected by validation-weighted AIC- and BIC-type criteria, and predictions are averaged across replicates to stabilize fits near the interpolation boundary. In addition to the core SVEM engine, the package provides deterministic high-order formula expansion, a permutation-based whole-model test heuristic, and a mixture-constrained random-search optimizer that combines Derringer–Suich desirability functions, bootstrap-based uncertainty summaries, and optional mean-level specification-limit probabilities to generate scored candidate tables and diverse exploitation and exploration medoids for sequential fit–score–run–refit workflows. A simulated lipid nanoparticle (LNP) formulation study illustrates these tools, and simulation experiments based on sparse quadratic response surfaces benchmark SVEMnet against repeated cross-validated elastic-net baselines.

Keywords: SVEM; design of experiments; relaxed lasso; LNP; formulation optimization; desirability functions;

1. Introduction

Formulation optimization experiments in chemistry and biopharmaceutics often operate with limited runs, complex factor spaces (interactions, curvature, mixtures), and multiple responses of interest. In such small- N regimes, flexible models can be unstable: small changes in the construction of the training sample (for example, different train/validation splits or cross-validation folds) may yield noticeably different predictions and selected penalties [1]. Self-Validated Ensemble Models (SVEM) were proposed by Lemkus et al. [2] to mitigate this instability by drawing fractional random-weight (FRW) [3] bootstraps paired with anti-correlated validation weights and averaging predictions across resampled fits. The idea was first presented under the name “autovalidation” by Gotwalt and Ramsey [4] and has since been extended with a permutation-based whole-model testing heuristic [5] and nonlinear base learners such as neural networks in

*Corresponding author

Email address: `akar1@asu.edu` (Andrew T. Karl)

mixture experiments [6]. SVEM is primarily intended as a predictive surrogate-modeling tool rather than a hypothesis-testing procedure, in line with the broader “to explain or to predict” distinction of Shmueli [7].

SVEM has already been implemented in JMP Pro (with forward-selection and Lasso base learners) and a proprietary JMP add-in (using neural network base learners, [6]). However, many analysts work in R, and reproducible small-sample workflows benefit from an open-source implementation that can be scripted, versioned, and embedded in simulation and optimization pipelines. To this end, this paper introduces **SVEMnet**, an R package that implements SVEM with elastic-net and optional relaxed elastic-net base learners [8, 9, 10, 11]. In a relaxed fit, **glmnet** computes a penalized solution path indexed by the penalty parameter λ , identifies the active set at each λ , and then refits an unpenalized linear model on that active set, interpolating between penalized and unpenalized coefficients via a relaxation parameter $\gamma \in [0, 1]$. In the sparse Gaussian linear model studied by Meinshausen [10], the relaxed lasso reduces the shrinkage of non-zero coefficients and can achieve lower prediction error than the standard lasso. Simulations in Section 4 indicate that combining relaxed base learners with the SVEM FRW ensemble can further reduce out-of-sample prediction error for Gaussian responses, plausibly because the ensemble averages over the additional variance introduced by relaxation. In place of the validation-weighted sum of squared errors criterion (denoted **wSSE**) used in earlier SVEM work by Lemkus et al. [2], **SVEMnet** standardizes on heuristic, validation-weighted information-criterion analogs—a validation-weighted Akaike information criterion (AIC) analog (**wAIC**) and a validation-weighted Bayesian information criterion (BIC; Schwarz criterion) analog (**wBIC**), with **wAIC** the default for Gaussian responses and **wBIC** the default for binomial responses [12, 13, 14]. Flexible fits such as the lasso are known to behave poorly near the interpolation boundary, where the number of runs n approaches the full expansion dimension p_{full} (the total number of coefficients in the “full” linear model expansion, including the intercept), with “peaking” in out-of-sample error documented in small-sample classification and regression problems [15] and in lasso model selection [16]. Related analyses of the $p \gtrsim n$ interpolation setting in linear prediction underscore that performance can shift sharply near this boundary [17, 18]. In the simulations reported in Section 4, **wAIC** and **wBIC** avoid this peaking, whereas the loss-only **wSSE** selector exhibits a pronounced spike at $n \approx p_{\text{full}}$.

Self-Validated Ensemble Models have already seen practical use in industrial DOE and chemometric settings, including mixture–process workflows for lipid nanoparticle (LNP) formulations and other pharmaceutical and analytical applications [19, 20, 6, 21, 22, 23, 24, 25, 26, 27]. These applications motivate an implementation tailored to chemometric DOE. In particular, **SVEMnet** is designed to automate many of the steps in the SVEM-based mixture–process workflow for LNP formulation optimization described by Karl et al. [19]. **SVEMnet** supplies an open-source SVEM implementation over **glmnet** with validation-weighted AIC/BIC selectors, deterministic high-order full model expansions, a permutation-based whole-model test heuristic, and a mixture-constrained random-search scoring tool for multi-response desirability and candidate generation.

SVEMnet is intended for round-by-round iteration in small- N DOE: fit SVEM models on the current data; use the random-search optimizer to generate and score a feasible candidate set under mixture and process constraints; select a small number of high-score exploitation medoids and high-uncertainty exploration medoids; then run those settings, append the new data, and refit the models. The LNP formulation example

below illustrates this workflow [19, 5]. The sequential workflow is an iterate–append loop that alternates exploitation and exploration based on predictive uncertainty, rather than a full Gaussian-process-based Bayesian optimization scheme, which remains the standard choice when richer covariance structures and acquisition strategies are desired [28, 29].

SVEMnet can be used with any single-error-stratum experimental design in which individual runs can be treated as independent. However, the predictive performance of **SVEMnet** will naturally depend on design quality. For physical experiments we recommend optimal designs [30, 31], fast flexible space-filling designs [32], or U-Bridge designs [33] rather than the simple Latin hypercube samples [34] that are employed for computational expediency in the baseline simulations in Section 4. Because the FRW bootstrap treats experimental runs as the resampling units, SVEM is inherently a single-stratum procedure: split-plot and other multi-stratum designs with hierarchical variance components are not supported and would require substantial structural changes (e.g., hierarchical base learners and a different resampling unit). In **SVEMnet**, blocking or batch indicators may be included only as fixed additive effects.

The remainder of the paper is organized as follows. Section 2 details the **SVEMnet** modeling engine: SVEM background, the **glmnet** wrapper (including relaxed refits), deterministic expansion tools, the validation-weighted **wAIC/wBIC** selector, and the multi-response random-search optimizer. Section 3 illustrates the workflow on an LNP formulation example. Section 4 reports simulations, and the paper concludes with a summary and outlook. Technical specifics of the validation-weighted criterion appear in Appendix A. Supplementary robustness checks and diagnostics appear in Appendix B. Mixed-model multiple-comparison tables for simulation results appear in Appendix C.

2. SVEMnet modeling and multi-response optimization

2.1. Software overview

SVEMnet takes a user-specified model formula and dataset, generates fractional random-weight (FRW) train/validation splits, fits elastic-net or relaxed elastic-net paths with **glmnet** within each FRW replicate, selects a penalty (and, when applicable, a relaxed refit) via a validation-weighted information criterion, and averages predictions across replicates. The same deterministic expansion of the right-hand side can be reused across responses so that all models share a common design matrix. The package additionally provides a permutation-based whole-model test heuristic and a mixture-constrained random-search optimizer that scores and selects candidates for additional experimental runs.

The main exported functions are:

- **SVEMnet()**: fit Gaussian or binomial SVEM models under a specified formula and dataset, with optional relaxed base learners and FRW control;
- **bigexp_terms()** and **bigexp_formula()**: build and reuse deterministic high-order factorial and polynomial linear model expansions from a single list of main-effects;
- **svem_wmt_multi()**: run the permutation-based whole-model test (WMT) and obtain approximate p -values and importance multipliers for multiple responses;

- `svem_random_table_multi()`: generate feasible candidate settings under mixture and process constraints (candidate generation only);
- `svem_score_random()` and `svem_select_from_score_table()`: generate feasible candidate settings, score them via multi-response desirability, and select diverse optimal and exploration candidates;
- `svem_export_candidates_csv()`: export collections of candidate tables for laboratory execution or documentation.

2.1.1. Workflow overview and typical use

The within-replicate tuning procedure used to select $(\alpha, \gamma, \lambda)$ is summarized in Figure 1 (Section 2.4). **SVEMnet** embeds this core engine in a sequential loop: (i) specify the factor space and construct a deterministic expansion (optional); (ii) fit SVEM models to one or more responses; (iii) optionally run the permutation-based whole-model diagnostic (WMT; Section 2.5) to assess global signal; (iv) generate a feasible candidate set under mixture and process constraints; (v) score candidates via multi-response desirability and summarize high-score (exploitation) and high-uncertainty (exploration) settings using medoids; and (vi) run selected settings, append the new rows, and refit. The optional `wmt_score` column is treated as a diagnostic overlay rather than the primary optimization objective.

The remainder of this section explores these functions in more detail. Worked Gaussian and binomial examples are provided in the CRAN help pages (e.g., `?SVEMnet`).

2.2. SVEM background

SVEM draws B replicates using FRW sampling. For each replicate b and observation $i = 1, \dots, n$, training weights w_i^{train} and an anti-correlated validation copy w_i^{valid} are constructed from a shared $U_i \sim \text{Uniform}(0, 1)$ via

$$w_i^{\text{train}} = -\log U_i, \quad w_i^{\text{valid}} = -\log(1 - U_i), \quad (1)$$

following the FRW scheme for univariate analysis introduced by Xu et al. [3], which underpins the original SVEM extensions to penalized regression (and the introduction of the anti-correlated validation weights) by Gotwalt and Ramsey [4] and Lemkus et al. [2]. For each FRW replicate we then rescale both the training and validation weights to have mean one, $w_i \leftarrow w_i/\bar{w}$ for $w \in \{w^{\text{train}}, w^{\text{valid}}\}$, matching `glmnet`'s internal normalization of observation weights.

Given $(w^{\text{train}}, w^{\text{valid}})$ for replicate b , **SVEMnet** fits an elastic-net or relaxed elastic-net base learner to the FRW-weighted training sample under w^{train} , evaluates a collection of path points using a validation-weighted information criterion computed with w^{valid} (Section 2.4), and stores predictions from the selected path point. Overall SVEM predictions are obtained by averaging these bootstrap predictions across $b = 1, \dots, B$. Lemkus et al. [2] tuned penalties by validation-weighted SSE (`wSSE`); **SVEMnet** adopts the same FRW-and-ensemble structure but standardizes on validation-weighted AIC/BIC analogs—`wAIC` default for Gaussian responses; `wBIC` default for binomial responses.

Although we focus on Gaussian responses in the exposition and case study, the software also implements a binomial (logistic) variant. In that case, the elastic-net base learner is fit under an FRW-weighted

logistic log-likelihood, penalties are selected on the deviance scale, and ensemble predictions are formed by averaging bootstrap-member-predicted probabilities; Appendix A gives the corresponding criteria.

Related work by Lu and Anderson-Cook [35] adapts the SVEM FRW-based self-validation mechanism to define a self-validated mean squared prediction error (SVMSPE) for model comparison and pairs it with sequential non-uniform space-filling (NUSF) design augmentation that allocates more runs to regions where a small set of candidate models differ most in their predictions. In **SVEMnet**, the FRW validation losses instead feed validation-weighted AIC/BIC-type selectors within a given elastic-net SVEM model class, while sequential design is handled separately by the desirability-based random-search optimizer in Section 2.6.

2.3. Implementation note: a SVEM wrapper over *glmnet*

SVEMnet implements SVEM by wrapping the standard and relaxed elastic-net paths in *glmnet* [8, 36, 9, 11] with FRW train/validation weights (Section 2.2). For each FRW replicate b and each α in a user-specified grid (default $\alpha \in \{0.5, 1\}$), **SVEMnet** calls *glmnet* with training weights w^{train} , an intercept, and predictor standardization enabled. By default, **SVEMnet** uses relaxed paths for Gaussian responses and standard elastic-net paths for binomial responses.

Relaxation alters the usual bias–variance trade-off by reducing shrinkage after variable selection: individual relaxed fits can have lower bias but higher variance, especially near the interpolation boundary. In a SVEM ensemble, averaging across FRW replicates can partially stabilize this additional variability. Empirically, the Gaussian simulations in Section 4 favor relaxed SVEM fits, whereas the binomial simulations favor non-relaxed fits; we default to `relaxed = TRUE` for Gaussian and `relaxed = FALSE` for binomial responses. Appendix B.3 provides additional diagnostic summaries of selected (λ, γ) distributions and bias–variance behavior in representative Gaussian and binomial settings.

Within each replicate, **SVEMnet** treats each combination of α and penalty λ (and, when relaxed fits are enabled, each relaxed refit value γ) as a candidate path point. For a given *glmnet* fit, the λ path is traversed and, for relaxed fits, a small grid of γ values is considered. Each candidate $(\alpha, \lambda, \gamma)$ is evaluated on the FRW validation copy using the chosen validation-weighted criterion (`wAIC`, `wBIC`, or `wSSE`; Appendix A), and the combination that minimizes this criterion determines the selected coefficients for replicate b . These selected coefficients populate a bootstrap-by-parameter coefficient matrix.

For new data, the design matrix is rebuilt to match training, each replicate’s coefficients are applied, and the resulting bootstrap predictions are averaged—on the response scale for Gaussian models and, by default, on the probability scale for binomial models. For Gaussian models, an optional *debias* step fits a linear calibration $\text{lm}(y \sim \hat{y})$ on the training data and applies the resulting intercept and slope to ensemble predictions. Debiasing is off by default and is included mainly to match the JMP implementation, where it is always applied [37].

2.3.1. Deterministic expansion utilities

A practical convenience in **SVEMnet** is that the user lists main-effect predictors only once and lets the expansion utilities (`bigexp_terms()` and `bigexp_formula()`) deterministically build interaction and polynomial columns. The same specification can be reused across responses, guaranteeing identical design matrices,

stable column order, and reproducible comparisons. With `factorial_order = 2` and `polynomial_order = 2`, for example, the generated right-hand side includes all main effects, two-way interactions, and quadratic terms (and, optionally, partial-cubic terms of the form $I(X^2):Z$) without hand-writing products or powers; categorical factors are handled using the contrasts recorded for the training data. We also include any mixture factors in the full expansion rather than constructing Scheffé polynomials [38].

When blocking or covariate factors (e.g., Operator, day, plate, ambient temperature) are supplied via `blocking` in `bigexp_terms()`, these factors make an additive adjustment to the response surface and do not interact with the other study factors.

Discrete numeric predictors. Some process variables are recorded as numeric but are only feasible to run at a discrete set of levels (e.g., fixed pump settings or allowable N:P ratios). To avoid proposing unattainable intermediate settings in candidate generation and whole-model diagnostics, `SVEMnet` allows users to mark such predictors via the `discrete_numeric` argument in `bigexp_terms()` (which only affects the candidate recipe settings, not the SVEM model fit). The resulting specification records the allowed numeric support in the training data, and downstream tools (random candidate generation and WMT evaluation-set construction) restrict sampling to these observed levels.

Practical guidance on choosing expansion order. When the true response surface order is unknown, we recommend starting with a moderately rich expansion that is scientifically plausible (e.g., third-order polynomials with up to three-way interactions and partial cubic terms for mixture–process screening), and allowing the elastic-net SVEM fit to downselect. This “start wide, shrink down” strategy is consistent with the SVEM-based LNP workflow of Karl et al. [19] and is supported by the simulation results in Section 4, where mild over-specification is typically less harmful than gross under-specification. In practice we recommend: (i) fit a candidate expansion; (ii) examine actual-by-predicted diagnostics and predictive uncertainty; (iii) optionally apply WMT (Section 2.5) to assess global signal; and (iv) if results are unstable, compare two adjacent expansion orders (e.g., Orders 2 and 3) and check whether the top candidate sets and fitted predictions are materially changed. A simple candidate stability check is to re-run scoring under both expansions and report the overlap of top-ranked recipes and medoids (Appendix B.6).

2.4. Selection criterion

At each candidate path point within an FRW replicate—indexed by the elastic-net mixing parameter α , the penalty λ , and, when relaxed fits are used, a relaxation parameter γ —`SVEMnet` evaluates a validation loss on the anti-correlated FRW copy: a weighted sum of squared errors for Gaussian responses and a deviance-style loss (weighted negative log-likelihood) for binomial responses. We then add a penalty of the form $g k_\lambda$, where k_λ is the number of nonzero coefficients (including the intercept). Choosing $g = 0$ recovers the historical loss-only selector (`wSSE`); $g = 2$ and $g = \log(n_{\text{eff}}^{\text{adm}})$ give validation-weighted analogs of AIC (`wAIC`) and BIC (`wBIC`), respectively. Appendix A records the full expressions and defines the effective-size guardrail $n_{\text{eff}}^{\text{adm}}$ used with `wAIC` and `wBIC` to avoid near-interpolating path points. This admissibility guardrail is applied only for the information-criterion selectors (`wAIC`, `wBIC`); the loss-only `wSSE` selector evaluates all path points without this constraint. Figure 1 summarizes the algorithm.

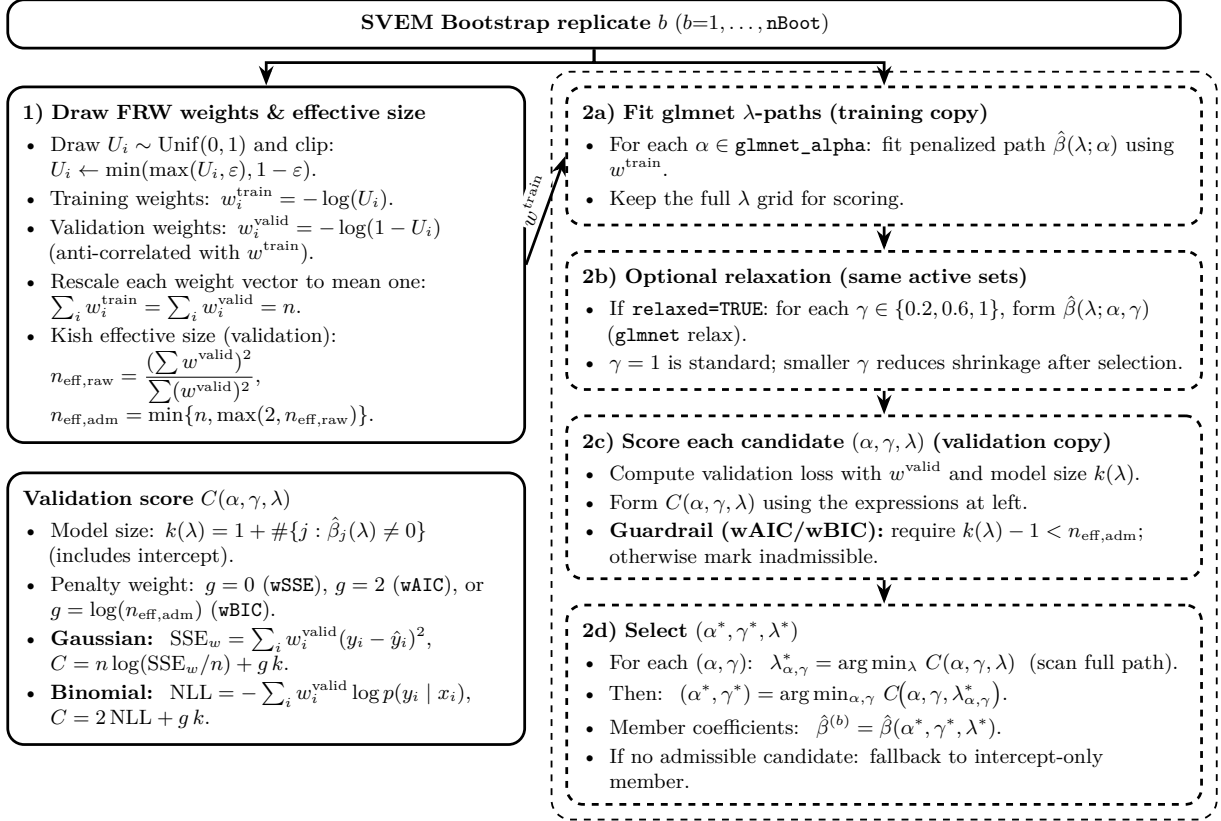


Figure 1: Within-replicate SVEMnet tuning flow for one bootstrap member b .

Because the FRW validation weights are random rather than fixed design weights, these scores are used heuristically for relative model comparison inside the FRW replicate rather than as exact AIC/BIC. As noted by Lu and Anderson-Cook [35], classical uses of AIC and BIC evaluate fit at the same observed locations used for estimation, which can lead to over-optimistic assessments. In **SVEMnet**, the **wAIC** and **wBIC** criteria are always computed on the FRW validation copy. For binomial models we retain the label **wSSE** even though the selector operates on the deviance scale rather than squared error.

Heuristic status and boundary behavior. Because the validation copy is itself random under FRW resampling, **wAIC** and **wBIC** are best interpreted as validation-weighted tuning scores rather than as classical information criteria with formal asymptotic guarantees. When $w_i^{\text{valid}} \equiv 1$ these criteria reduce (up to constants independent of λ) to the standard Gaussian AIC/BIC forms, and the use of $n_{\text{eff}}^{\text{adm}}$ in the BIC-style penalty can be viewed as a simple effective-size adjustment for highly variable validation weights. Empirically, the primary motivation for **wAIC** and **wBIC** in SVEM is stability near the interpolation boundary $n \approx p_{\text{full}}$. Appendix B.1 provides a focused simulation around $n = p_{\text{full}}$ that compares **wAIC/wBIC** with the loss-only **wSSE** selector in terms of selected model size and out-of-sample error.

2.5. Permutation-based whole-model diagnostic (WMT)

SVEMnet includes a permutation-based whole-model test (WMT) heuristic for Gaussian SVEM fits [5]. The goal is to provide a practical diagnostic for whether a fitted SVEM model exhibits global factor signal beyond what would be expected under a constant-response null, complementing the usual actual-

by-predicted and residual plots. WMT is a randomized, simulation-based procedure and the resulting “ p -values” are approximate; we treat them as diagnostic summaries rather than as formal hypothesis tests.

At a high level, WMT compares standardized SVEM predictions on a space-filling set of evaluation points with a reference distribution obtained by refitting the same SVEM specification to permuted responses. Let $T = \{x_i\}_{i=1}^{n_{\text{point}}}$ be a space-filling set over the modeled factor space (respecting mixture constraints, categorical levels, and any recorded discrete numeric supports). For each evaluation point $x \in T$, we compute a standardized prediction

$$h(x) = \frac{\hat{f}(x) - \bar{y}}{\hat{s}(x)}, \quad (2)$$

where $\hat{f}(x)$ is the SVEM ensemble mean prediction, \bar{y} is the training-set mean response, and $\hat{s}(x)$ is the ensemble standard deviation across SVEM bootstrap predictions at x (a pointwise uncertainty proxy) [5]. Repeating this calculation for n_{SVEM} independent SVEM refits (new FRW weights each time) yields an $n_{\text{SVEM}} \times n_{\text{point}}$ matrix of standardized predictions. WMT then fits the same SVEM specification to n_{perm} random permutations of the response vector and records the corresponding standardized predictions on T in an $n_{\text{perm}} \times n_{\text{point}}$ reference matrix.

To summarize global deviation from the null, WMT standardizes the permutation matrix columnwise, applies a reduced-rank singular value decomposition (retaining the leading components explaining a user-specified fraction of the permutation variance), and computes Mahalanobis-like distances for the permutation rows and for the original-data refits, following Karl [5]. The resulting distance distributions are displayed graphically; clear separation indicates strong global signal. For a scalar summary, **SVEMnet** fits a flexible parametric distribution to the permutation distances (SHASH [39]) and reports the fitted right-tail probability as a whole-model “ p -value.” Because the procedure uses finite budgets (n_{perm} , n_{point} , n_{SVEM}), results have Monte Carlo variability; for interpretability, users should set and report random seeds and treat marginal cases cautiously. The current **SVEMnet** defaults are $n_{\text{point}} = 2000$, $n_{\text{SVEM}} = 10$, $n_{\text{perm}} = 150$, and a 90% variance-retention threshold for the reduced-rank distance calculation.

In **SVEMnet**, WMT can be run for multiple responses via `svem_wmt_multi()`, which reuses a shared deterministic expansion and constraint specification. The resulting WMT “multipliers” (monotone transforms of the per-response approximate p -values) can optionally reweight user-specified multi-response desirability weights when producing the diagnostic `wmt_score` column (Section 2.6). In this paper we treat WMT reweighting as a secondary sensitivity check rather than as the primary decision rule, consistent with the diagnostic intent of the test heuristic.

2.6. Random-search scoring and candidate selection for multi-response design

The built-in stochastic optimizer implements the desirability-based generate-and-rank strategy sketched in the introduction. Starting from fitted **SVEMnet** models, it generates feasible candidate settings under the observed factor ranges and user-specified mixture constraints, evaluates each setting via a multi-response desirability score, and returns shortlists of high-score (exploitation) and high-uncertainty (exploration) candidates. The following subsections describe candidate generation and mean-level specification probabilities, construction and weighting of desirability scores, the uncertainty measure used to target exploration, and the medoid-based selection of diverse recipes.

2.6.1. Sampling and specification limits

Candidate settings are generated by `svem_random_table_multi()` and, in typical use, `svem_score_random()` calls this generator and then appends SVEM-based predictions, desirability scores, uncertainty summaries, and (optionally) mean-in-specification proxies. When specification limits are provided for a response, **SVEMnet** uses the SVEM bootstrap to estimate, at each candidate, the probability that the *process mean* lies inside those limits and adds per-response and joint mean-level specification probabilities (e.g., `prob_in_spec` and `p_joint_mean`) as additional columns in the scored table. These mean-level probabilities are used only as ranking proxies: formal specification limits apply to individual observations, not to the process mean.

2.6.2. Scoring and response weighting

For each response r , we map predictions to unit-interval desirabilities $d_r(x) \in [0, 1]$ using Derringer–Suich curves and form a multi-response score as a weighted geometric mean of the per-response desirabilities,

$$S(x) = \exp\left(\sum_r w_r \log(d_{r,\varepsilon}(x))\right), \quad d_{r,\varepsilon}(x) = (1 - \varepsilon) d_r(x) + \varepsilon. \quad (3)$$

using a small ε (default 10^{-6}) to avoid $\log(0)$ [40, 41, 30].

Practical desirability calibration and sensitivity checks. In practice we recommend choosing Derringer–Suich parameters from scientific acceptability ranges rather than from the fitted model itself. For each response, the user specifies a goal (maximize, minimize, or hit a target) together with bounds and optionally a target. The bounds define where desirability is essentially zero (clearly unacceptable) and where it saturates at one (fully acceptable or “good enough”); the shape exponent controls how rapidly desirability approaches one between these values. **SVEMnet** uses a simple default shape (exponent = 1) unless the user supplies custom exponents, which yields a linear ramp on the response scale. Exponents greater than one make the desirability curve more stringent near the target, while exponents below one make it more tolerant.

The weighted geometric mean in (3) is used because it is the standard aggregation in the desirability literature and because it enforces “weakest-link” behavior: if any key response has near-zero desirability, the overall score is driven toward zero, reflecting the fact that a single out-of-spec response can invalidate a recipe [41]. Alternatives such as arithmetic means can mask poor performance in a critical response.

When desirability parameters encode subjective trade-offs, simple sensitivity checks are valuable. A practical approach is to rerun scoring under plausible alternative bounds, targets, exponents, or response weights and then compare the overlap and rank stability of the top candidates and medoids. Appendix B.5 provides a compact desirability-calibration sensitivity check.

User-specified goal weights \tilde{w}_r are first normalized to \bar{w}_r with $\sum_r \bar{w}_r = 1$. When `reweight_by_wmt = FALSE`, we set $w_r = \bar{w}_r$ and report a single column `score` based on $S(x)$. When `reweight_by_wmt = TRUE` for Gaussian responses, we further reweight the normalized user weights by a monotone function of the permutation whole-model p -values from [5] (for example $-\log_{10}(p_r)$), renormalize to obtain WMT-adjusted weights w_r^{WMT} , and compute a second geometric-mean score `wmt_score` by using $w_r = w_r^{\text{WMT}}$ in $S(x)$. These WMT-adjusted weights are diagnostic and do not alter the underlying SVEM fits. In this paper we treat the resulting WMT-based multipliers as a secondary priority: the primary optimization uses

the user-specified weights \tilde{w}_r , and `wmt_score` is intended to provide additional, lower-priority optimal candidates when budget allows.

Thus the output table always contains `score`, based purely on the user-specified weights \tilde{w}_r , and, when applicable, an additional `wmt_score` column that augments those weights using the WMT results. Gaussian and binomial outcomes are handled on the same scale by applying desirability functions to predicted means and predicted probabilities, respectively.

For candidate scoring, `blocking` variables are held fixed at a single reference setting while the controllable factors are varied over the feasible region. Categorical blocking factors are evaluated at the most common observed level, and continuous blocking covariates are evaluated at the midpoint of their modeled range. Under the additive-only blocking assumption this defines a consistent reference for comparing controllable settings; if desirability bounds/targets are specified on an absolute response scale, users may optionally re-score at alternative blocking levels to confirm stability of the top candidates.

2.6.3. Uncertainty and exploration

For each response r we compute a percentile prediction interval $[\ell_r(x), u_r(x)]$ at level $1 - \alpha$ from the SVEM bootstrap and define the interval width $W_r(x) = u_r(x) - \ell_r(x)$. To place uncertainty on a comparable scale across responses, we normalize $W_r(x)$ using the empirical 2%–98% range for that response and aggregate the normalized widths using the original normalized goal weights \bar{w}_r :

$$U(x) = \sum_r \bar{w}_r \text{Norm}_{0,1}(W_r(x); q_{r,0.02}, q_{r,0.98}). \quad (4)$$

where $\text{Norm}_{0,1}(\cdot; q_{r,0.02}, q_{r,0.98})$ denotes a rescaling to $[0, 1]$ based on the empirical 2% and 98% quantiles $q_{r,0.02}$ and $q_{r,0.98}$ for response r . Large values of $U(x)$ correspond to regions of higher predicted uncertainty. We report the single exploration target $\arg \max_x U(x)$ and also use $U(x)$ to construct exploration shortlists in the next subsection.

2.6.4. Diverse candidates via medoids and practical defaults

Score and uncertainty surfaces often exhibit ridges of near-equivalent values across a broad range of factor settings. To capture this range of feasible recipes with similar predicted performance, the user may choose a number k of candidates by ranking the scored table on a scalar objective (typically $S(x)$ or $U(x)$, corresponding to the `score` and `uncertainty_measure` columns, but also, for example, `wmt_score`, `p_joint_mean`, or any other numeric column), retaining either the top fraction or the top n rows, and clustering this subset using Gower distance on the predictor columns with partitioning-around-medoids (PAM) [42, 43]. The medoids are existing feasible rows and summarize diverse “exploitation” and “exploration” recipes, and the functions `svem_score_random()` and `svem_select_from_score_table()` additionally return the single best row under the chosen objective. Figure 2 illustrates this strategy for the central composite design from Table 6.8 of Myers et al. [30].

3. Example LNP Application

We illustrate the workflow using the bundled simulated LNP formulation screening data, which include four mixture components (PEG, Helper, Ionizable, Cholesterol), a categorical ionizable lipid type, two

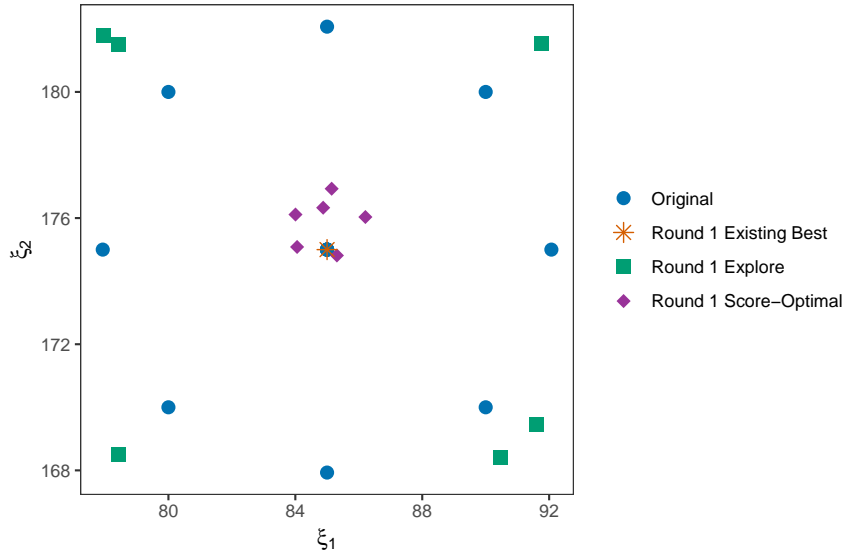


Figure 2: Original CCD runs from Table 6.8 of Myers et al. [30] (blue circles), SVEMnet-selected optimal candidates (purple diamonds), and high-uncertainty exploration runs (green squares) for the y_1 response, which attains its maximum near the center of the design region.

discrete numeric process factors (`N_P_ratio` and `flow_rate`), a categorical Operator factor, and three responses: Potency, Size, and PDI. This example parallels the SVEM-based mixture-process LNP workflow of Karl et al. [19].

We first build a single deterministic right-hand-side expansion and reuse it across all three models. We treat Operator as a blocking variable that enters additively and does not interact with other study factors.

```

1 library(SVEMnet)
2 data(lipid_screen)
3 spec <- bigexp_terms(
4   Potency ~ PEG + Helper + Ionizable + Cholesterol +
5     Ionizable_Lipid_Type + N_P_ratio + flow_rate,
6   blocking      = "Operator", # additive blocking factor
7   discrete_numeric = c("N_P_ratio","flow_rate"),
8   data          = lipid_screen,
9   factorial_order = 3, # up to 3-way interactions
10  polynomial_order = 3, # up to cubic terms
11  include_pc_2way = TRUE
12 )
13 form_pot <- bigexp_formula(spec, "Potency")
14 form_siz <- bigexp_formula(spec, "Size")
15 form_pdi <- bigexp_formula(spec, "PDI")

```

Using this shared expansion for a third-order model, we fit Gaussian SVEM models for each response with default settings and collect them in a named list. Multi-response goals are set so that Potency is maximized, while Size and PDI are minimized, and mixture constraints reflect practical bounds and a unit-sum constraint on the four composition variables:

```

1 set.seed(1)
2 fit_pot <- SVEMnet(form_pot, lipid_screen)

```

```

3 fit_siz <- SVEMnet(form_siz, lipid_screen)
4 fit_pdi <- SVEMnet(form_pdi, lipid_screen)
5
6 objs <- list(Potency = fit_pot, Size = fit_siz, PDI = fit_pdi)
7
8 goals <- list(
9   Potency = list(goal = "max", weight = 0.6),
10  Size     = list(goal = "min", weight = 0.3),
11  PDI      = list(goal = "min", weight = 0.1)
12 )
13
14 mix <- list(list(
15   vars = c("PEG", "Helper", "Ionizable", "Cholesterol"),
16   lower = c(0.01, 0.10, 0.10, 0.10),
17   upper = c(0.05, 0.60, 0.60, 0.60),
18   total = 1.0
19 ))

```

3.1. Whole-model reweighting and permutation tests

To assess which responses show the strongest relationship with the study factors, we apply the permutation-based whole-model test heuristic (WMT) of Karl [5] to each SVEM model. WMT-based multipliers can optionally reweight the user-specified response weights, prioritizing responses with stronger predictive signal and down-weighting weaker ones. Consistent with Karl [5], we view these results as a way to highlight responses with clearer global signal, not as a hard filter: in small or noisy studies the WMT heuristic can have limited power, so candidate sets should not be chosen solely by appealing to WMT p -values or multipliers. Because WMT is permutation-based with finite simulation budgets, these p -values are approximate.

The helper `svem_wmt_multi()` runs the permutation test for each response under the shared deterministic expansion and mixture constraints, and returns approximate p -values and multipliers:

```

1 set.seed(123)
2 wmt_out <- svem_wmt_multi(
3   formulas      = list(Potency = form_pot,
4                        Size     = form_siz,
5                        PDI      = form_pdi),
6   data          = lipid_screen,
7   mixture_groups = mix,
8   wmt_control   = list(seed = 123)
9 )
10 wmt_out$p_values
11 wmt_out$multipliers

```

The approximate whole-model p -values under the default permutation budget were Size $p \approx 1.0 \times 10^{-16}$, Potency $p \approx 4.1 \times 10^{-9}$, and PDI $p \approx 0.77$. Thus Size and Potency show strong global signal, whereas PDI does not (although lack of signal in this heuristic alone should not be used to conclude that there is no relationship between the study factors and PDI [5]). Figure 3 shows the associated whole-model significance diagnostic, generated by `svem_wmt_multi()` under the shared expansion and mixture constraints.

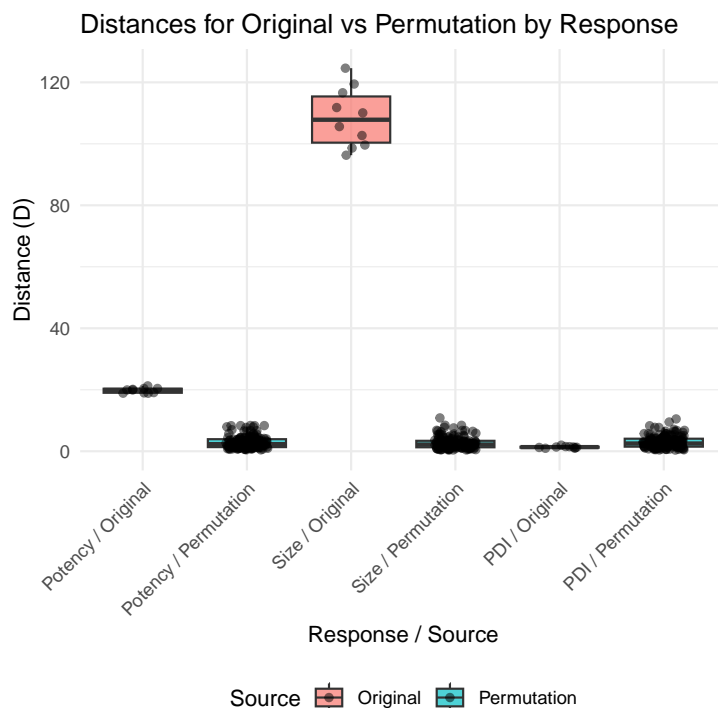


Figure 3: Whole-model significance diagnostic (WMT) for Potency, Size, and PDI: distance distributions for the original data versus permuted fits under the shared expansion and mixture constraints.

Clear separation between the “Original” and permutation-based distance distributions indicates strong global factor signal, as in Figure 3 of Karl [5]. Appendix B.4 reports a simple stability check over random seeds and permutation budgets for this example.

3.2. Random-search scoring, candidate selection, and sequential use

To illustrate the optional specification-limit handling, we impose mean-level requirements on the three responses—limits on the predicted process means rather than on individual unit-level measurements: $Potency > 78$, $Size < 100$, and $PDI < 0.25$. Only the bounded side of each limit needs to be supplied:

```

1 specs_ds <- list(
2   Potency = list(lower = 78),
3   Size    = list(upper = 100),
4   PDI     = list(upper = 0.25)
5 )

```

The random-search scoring step then evaluates a large number of feasible settings (default 25,000). For each candidate, `svem_score_random()` evaluates the SVEM models, computes per-response Derringer–Suich desirabilities, aggregates them into a single multi-response score via a weighted geometric mean, constructs a scalar uncertainty measure $U(x)$ from bootstrap percentile intervals, and, when specifications are supplied, computes mean-level probabilities that each candidate’s modeled mean lies inside the user limits. Supplying `wmt = wmt_out` adds a WMT-adjusted score column `wmt_score` in addition to the user-weighted score:

```

1 set.seed(3)
2 scored <- svem_score_random(
3   objects      = objs,

```

```

4 goals      = goals,
5 data       = lipid_screen,
6 mixture_groups = mix,
7 wmt        = wmt_out, # optional: NULL for no WMT
8 specs      = specs_ds # optional: NULL for no design-space columns
9 )

```

From the resulting scored table we extract high-score, exploration, and design-space candidates using `svem_select_from_score_table()`. For example, the following call selects five near-optimal score medoids, in addition to the single highest scored recipe from the candidate set of 25,000:

```

1 # Score-optimal medoids (user-weighted score)
2 opt_sel <- svem_select_from_score_table(
3   score_table = scored$score_table,
4   target      = "score",
5   direction   = "max",
6   k           = 5,
7   top_type    = "frac",
8   top         = 0.1,
9   label       = "round1_score_optimal"
10 )

```

Analogous calls with `target = "uncertainty_measure"` and `target = "p_joint_mean"` (and `score_table` set to either the random-search candidates or the original screening runs) were used to obtain the candidates summarized in Tables 1 and 2. The replication script contains the full set of `svem_select_from_score_table()` calls [44]. Candidate tables for laboratory use can be exported with `svem_export_candidates_csv()`; the Supplementary CSV file was generated using this function and is included in the Mendeley Data archive [44].

Tables 1 and 2 show four SVEM candidates from the simulated first-round lipid screening. The first row corresponds to the best existing screened run by multi-response score and provides a baseline. This row displays the original level of the `blocking` factor, `Operator`, which may differ from the level shown for the random-search candidates; the latter are evaluated at the reference `Operator` level used for scoring. The additive offsets for the `Operator` levels are visible in the fitted coefficients (e.g., `coef(fit_pot)`), and predictions for other `Operator` levels can be obtained via `predict(fit_pot, newdata = ...)`. The score-optimal run from the random search trades a modest reduction in predicted Potency for a large improvement in Size, yielding an overall desirability of one. In this example, the `wmt_score` optimum coincides with the score-optimal run, so no additional row is shown. The “In-spec” optimum illustrates a candidate that lies comfortably inside the specification region. The exploration target has the highest uncertainty measure $U(x)$ and sits near the edge of the feasible mixture region, with poor predicted Potency. Table 2 reports the SVEM point predictions together with the primary desirability score (`score`), the WMT-reweighted diagnostic score (`wmt_score`), the mean-in-spec proxy $p_{\text{joint,mean}}$, and the uncertainty measure $U(x)$ (Section 2.6).

Table 1: Representative SVEM candidate recipes from the lipid screening example. Mixture components are proportions on the 0–1 scale; process factors are in their native units. All random-search candidates are evaluated at the reference (modal) Operator level A.

Scenario	PEG	Helper	Ionizable	Cholesterol	Ionizable Type	N:P	flow rate	Operator
Best screened	0.047	0.430	0.140	0.383	H101	6	2.5	B
Max Score	0.048	0.583	0.110	0.259	H101	10	2.5	A
In-spec	0.040	0.458	0.165	0.337	H103	14	2.5	A
Exploration	0.011	0.592	0.123	0.273	H103	6	2.5	A

Table 2: Predicted behavior for the candidate recipes in Table 1. Responses are SVEM point predictions.

Scenario	Potency	Size	PDI	score	wmt_score	$p_{\text{joint,mean}}$	$U(x)$
Best screened	91.5	88.2	0.21	0.83	0.88	0.93	0.77
Max Score	89.1	50.4	0.17	1.00	1.00	1.00	0.39
In-spec	84.9	76.5	0.17	0.83	0.82	1.00	0.73
Exploration	74.3	51.2	0.20	0.45	0.54	0.09	0.94

3.3. Computational environment and runtime

All timings were obtained on a Windows 11 x64 desktop with an Intel Core Ultra 7 265 CPU (20 cores, 2.4 GHz) and 64 GB RAM, running R 4.5.2 with **SVEMnet** 3.2.0 and **glmnet** 4.1-10 and parallel execution enabled for the WMT. Users should note that on Windows, parallelization of the WMT may trigger a one-time Windows Firewall prompt for R when worker processes are created; this is due to local socket connections between R processes and does not involve external network access. In typical setups the computation will still run if the prompt is dismissed.

For the lipid screening example (23 experimental runs, three Gaussian responses, shared third-order deterministic expansion, and a 25 000-point random candidate set), a single end-to-end run of the workflow required about 260 seconds: roughly 92 seconds to fit **SVEMnet** for the three responses, 156 seconds for the optional permutation-based whole-model tests, and 9 seconds for the random-search scoring, candidate selection, and CSV export. Thus most of the computational cost lies in SVEM model fitting and the WMT; the optimization layer is comparatively light.

4. Simulation study

We carried out simulations comparing **SVEMnet** to repeated cross-validated elastic-net baselines over grids of sample sizes and signal strengths, where “signal strength” refers to the proportion of variance in the data explained by the underlying model (target R^2). The baselines use a wrapper `glmnet_with_cv()` around `cv.glmnet`, matching the α grid and penalty path to the **SVEMnet** settings. For each configuration we ran both the default two-point grid $\alpha \in \{0.5, 1\}$ and a lasso-only grid $\alpha = 1$, which behaved indistinguishably in these simulations. All simulation scripts and CSV result files are provided in the replication bundle of Karl [44].

4.1. Design and metrics

Each replicate uses a sparse quadratic response surface in four continuous factors $X_1:X_4 \in [-1, 1]$ and one three-level factor $X_5 \in \text{L1, L2, L3}$ (sum-to-zero coding). Training data are Latin hypercube samples for $X_1:X_4$ with balanced X_5 levels [34], with $n_{\text{total}} \in \{15, 20, \dots, 50\}$. As noted in the introduction, we use Latin hypercubes here for simulation convenience; in practice, more sophisticated optimal or space-filling designs are typically preferable when constructing the initial experimental design [45, 30, 32, 33, 31]. Appendix B.2 reports representative robustness checks using a face-centered central composite design (CCD) in place of the Latin-hypercube baseline and using denser/alternative coefficient regimes. All simulations treat runs as independent (single error stratum); hierarchical split-plot dependence is outside the scope of SVEM and is not considered.

The quadratic model has $p_{\text{full}} = 25$ parameters (including the intercept), so $n_{\text{total}} = p_{\text{full}} = 25$ is the interpolation boundary. To induce sparsity, in each simulation replicate and for each coefficient j , draw $\pi_j \sim \text{Beta}(0.5, 0.5)$, $Z_j \sim \text{Bernoulli}(\pi_j)$, and E_j from a mean-zero Laplace distribution, and set $\beta_j = Z_j E_j$. This produces many exact zeros with Laplace-distributed nonzero effects.

For the Gaussian case, we evaluate the noiseless response surface $f(x)$ on a large space-filling grid to estimate its domain-scale standard deviation $\sigma_f = \text{sd}\{f(x)\}$. We then add Gaussian noise to the training responses using

$$Y = f(x) + \varepsilon, \quad \varepsilon \sim \mathcal{N}(0, \sigma_\varepsilon^2), \quad \sigma_\varepsilon = \sigma_f \sqrt{\frac{1 - R^2}{R^2}},$$

so that $\text{Var}\{f(x)\}/(\text{Var}\{f(x)\} + \text{Var}(\varepsilon)) \approx R^2$ matches a target $R^2 \in \{0.5, 0.9\}$. All methods are scored on a separate noiseless 10,000-point holdout. Performance is summarized by the normalized RMSE, $\text{NRMSE} = \text{RMSE}/\text{sd}\{f(x)\}$ (with $\text{sd}\{f(x)\}$ computed on the holdout grid), and we report $\log_e(\text{NRMSE})$.

To probe under- and over-specification, we fit three right-hand-side expansions against the same data-generating mechanism (whose true order is quadratic): *Order 1* = main effects only (underspecified), $p_{\text{full}} = 7$; *Order 2* = quadratics and two-way interactions (correct order), $p_{\text{full}} = 25$; and *Order 3* = Order 2 plus all three-way interactions and pure cubic terms (overspecified), $p_{\text{full}} = 45$. Within each expansion, we compare **SVEMnet** objectives (**wSSE**, **wAIC**, **wBIC**) with and without relaxed base learners, and repeated $5 \times \text{CV}$ elastic-net baselines using the same α grids.

The binomial study uses the same latent quadratic surface $\eta(x)$ but treats the binary outcome as a discretized analog. We define $p(x) = \text{logit}^{-1}(s \eta(x))$ with $s = \sqrt{R^2/(1 - R^2)}$ for $R^2 \in \{0.5, 0.9\}$, draw training labels $Y \sim \text{Bernoulli}\{p(x)\}$ once per replicate, and score models on a large noiseless holdout using the true probabilities $p(x)$. Here R^2 serves as a convenient signal-strength parameter (an approximate analog of the Gaussian-domain R^2 rather than an exact GLM coefficient of determination). Performance is measured by holdout log-loss. Methods again include **SVEMnet** with $\{\text{wAIC}, \text{wBIC}, \text{wSSE}\}$ and repeated cross-validated baselines matched on α and relaxation.

To reduce Monte Carlo error, the summary curves in Figures 4, 5, and 6 average over 1000 independent simulation replicates for each combination of n_{total} , target R^2 , model order, and fitting method (**Setting**). In these overview plots we fix a common set of tuning defaults. For Gaussian responses, `cv.glmnet` uses standard (non-relaxed) elastic-net paths (`relax = FALSE`) and **SVEMnet** uses relaxed base learners (`relax = TRUE`); post-hoc debiasing is disabled for all methods and the elastic-net mixing grid is held at $\alpha \in \{0.5, 1\}$.

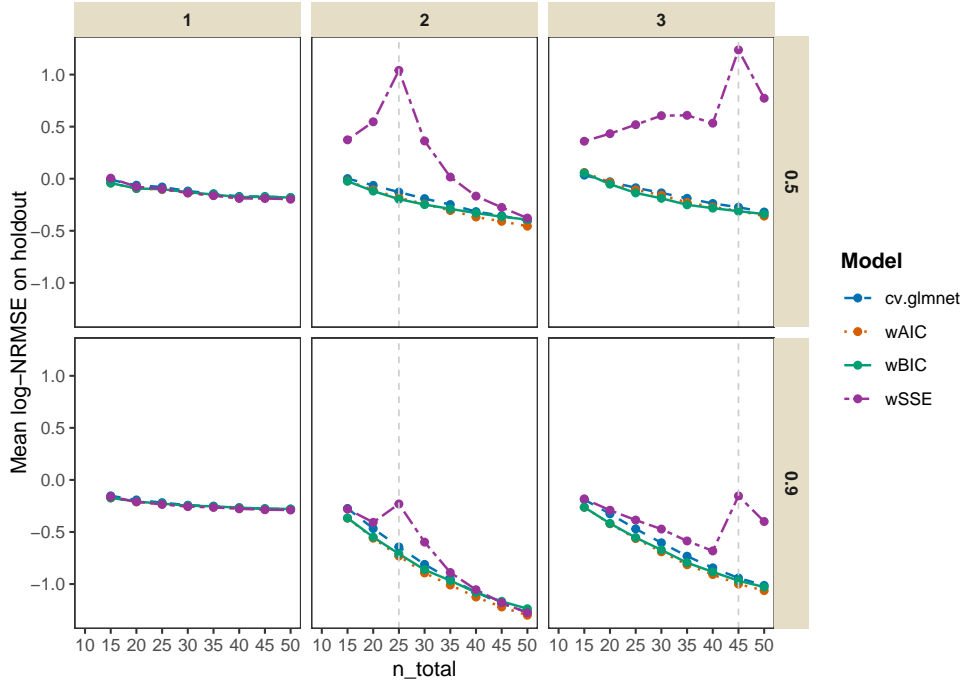


Figure 4: Gaussian simulations: mean holdout log-NRMSE (lower is better) versus n_{total} by target R^2 (rows) and fitted expansion order (columns). Vertical lines mark interpolation boundaries $n_{\text{total}} = p_{\text{full}}$.

For binomial responses, all methods use non-relaxed paths (`relax = FALSE`) with the same default α grid. These settings are used for all model orders shown in the figures.

For the mixed-model multiple-comparison summaries in Tables C.6 and C.7 we focus on the correctly specified quadratic expansion (Order 2) and explore a richer grid of SVEM and `cv.glmnet` configurations. Separate simulation runs with 250 (Gaussian) and 200 (binomial) independent replicates for each combination of n_{total} , `Target_R2`, and `Setting` are used to fit linear mixed models with `Setting` as the primary fixed effect, n_{total} , `Target_R2`, and their interaction as additional categorical fixed effects, and a random intercept for replicate (`RunID`). Pairwise differences in log-NRMSE and log-loss are summarized via Tukey–Kramer all-pairs comparisons of the model-based least-squares means. The loss-only `wSSE` selector is included in the simulation runs and overview figures but excluded from the mixed-model datasets to avoid inflating the number of clearly noncompetitive comparisons. The resulting connecting-letter displays appear in Tables C.6 and C.7 and in the Supplement.

4.2. Gaussian results

Several consistent patterns emerge across R^2 levels, sample sizes, and model orders.

Figure 4 summarizes mean log-NRMSE on a large noiseless holdout as a function of n_{total} for target $R^2 \in \{0.5, 0.9\}$ (rows) and three right-hand-side expansion orders (columns). Curves compare repeated 5×CV elastic-net baselines (`cv.glmnet`) with SVEMnet selectors (`wAIC`, `wBIC`, and the historical loss-only `wSSE`). For these overview plots, `cv.glmnet` uses standard (non-relaxed) elastic-net paths, SVEMnet uses relaxed base learners for Gaussian responses, and post-hoc debiasing is disabled for all methods.

To connect predictive error to selected model complexity, Figure 5 reports the mean of the within-replicate median active-set size k_λ (number of nonzero coefficients) selected across SVEM bootstrap

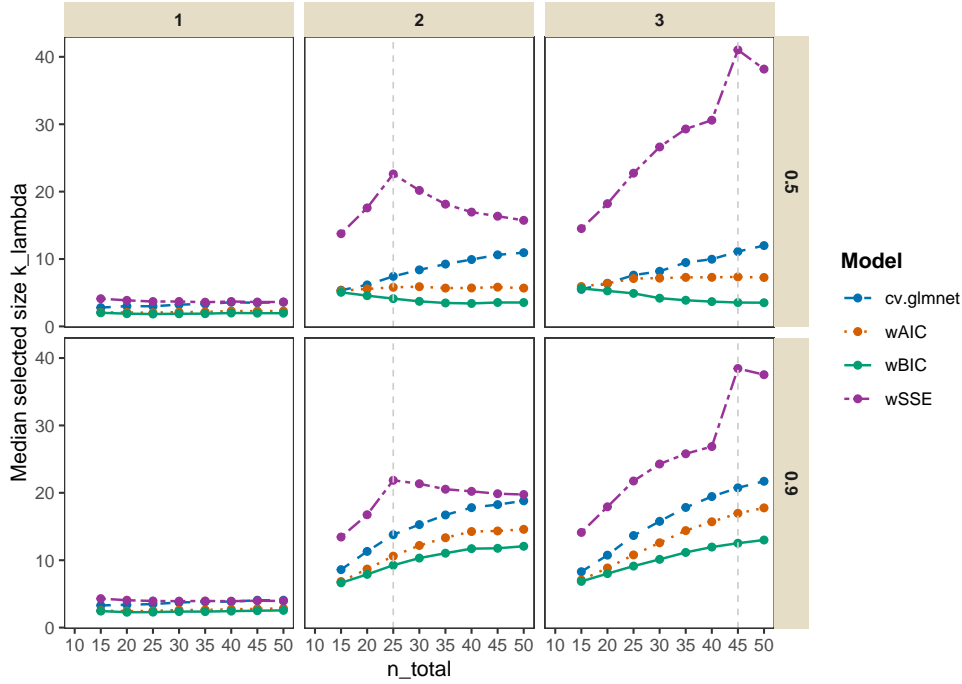


Figure 5: Gaussian simulations: mean selected model size (median k_λ across SVEM replicates) versus n_{total} by target R^2 (rows) and expansion order (columns). Vertical lines mark $n_{\text{total}} = p_{\text{full}}$.

replicates. The loss-only **wSSE** selector shows a pronounced spike near $n_{\text{total}} = p_{\text{full}}$, whereas **wAIC** and **wBIC** remain stable.

- Information criteria versus loss-only selectors.** Across the grid, **SVEMnet** with validation-weighted information criteria (**wAIC**, **wBIC**) consistently outperforms the historical loss-only **wSSE** selector in mean holdout log-NRMSE. Relative to repeated **cv.glmnet**, **SVEMnet-wAIC** is typically best or tied for best for the correctly specified and mildly overspecified expansions (Orders 2 and 3), with **wBIC** close behind (Figure 4 and Appendix Table C.6).
- Relaxation and debiasing.** For **SVEMnet** under **wAIC/wBIC**, enabling relaxed base learners improves holdout performance in the Gaussian setting, whereas relaxation tends to degrade the repeated **cv.glmnet** baselines. The optional post-hoc debiasing step ($y \sim \hat{y}$ fit on the training data) does not improve mean holdout error in these simulations and is mildly unfavorable on average, so we recommend `debias = FALSE` as the default for Gaussian responses (Table C.6).
- Effect of expansion order.** Underspecification (Order 1, main effects only) substantially degrades accuracy. The correctly specified quadratic expansion (Order 2) performs best, and mild overspecification with additional three-way interactions and pure cubic terms (Order 3) degrades far less than underspecification (Figure 4).
- Peaking near the interpolation boundary.** For each simulation run we recorded k_{median} , the median number of active parameters k_λ across SVEM bootstrap replicates; Figure 5 shows the mean of these medians over simulation replicates. The **wSSE** selector shows a pronounced spike in both mean log-NRMSE (Figure 4) and median selected model size k_λ (Figure 5) when n_{total} equals the

expansion dimensions: $p_{\text{full}} = 25$ for Order 2 and $p_{\text{full}} = 45$ for Order 3 ($p_{\text{full}} = 7$ for Order 1 is not included in the range of the graph). This is the “peaking” phenomenon near the interpolation boundary in small-sample regression [16]. In contrast, **wAIC** and **wBIC** – with their effective sample size guardrails – remain smooth in both error and k_λ .

Overall, the simulations support the default configuration used in **SVEMnet** for Gaussian responses: validation-weighted **wAIC**, relaxed elastic-net base learners, **debias = FALSE**, and $\alpha \in \{0.5, 1\}$.

4.3. Binomial results

Across $n_{\text{total}} \in \{15, \dots, 50\}$ and $R^2 \in \{0.5, 0.9\}$, non-relaxed fits dominate their relaxed counterparts on the holdout log-loss scale. For the correctly specified quadratic expansion (Order 2), **SVEMnet** with **wBIC** and the non-relaxed repeated-cv **glmnet** baselines perform similarly: Tukey–Kramer comparisons based on the mixed-effects model place these configurations in the same best-performing group (Table C.7). However, Figure 6 suggests that **SVEMnet** with **wBIC** may outperform **cv.glmnet** in the overspecified case.

Relaxed refits are systematically worse: for each objective and α grid the **relax = TRUE** versions have larger least-squares means, with the relaxed cross-validated baselines forming the worst group in Table C.7. The degradation from relaxation is especially pronounced for the repeated-cv **glmnet** fits, where the increase in mean log-loss is roughly twice as large as for the corresponding **SVEMnet** selectors.

Allowing $\alpha \in \{0.5, 1\}$ has no material impact relative to lasso-only fits ($\alpha = 1$): default two-point grids and pure lasso grids are indistinguishable within each selection method. As in the Gaussian case, the loss-only **wSSE** selector (included only in the overview plots) exhibits a pronounced error spike at $n_{\text{total}} = p_{\text{full}}$, now on the log-loss scale (Figure 6). **SVEMnet** with **wAIC** underperforms **wBIC** in the binomial setting. These simulations support the default configuration used in **SVEMnet** for binomial responses: validation-weighted **wBIC**, no relaxation, and $\alpha \in \{0.5, 1\}$.

Figure 6 summarizes the corresponding mean holdout log-loss curves for the overview settings (all methods non-relaxed; default α grid).

5. Conclusion

SVEMnet provides an open-source implementation of Self-Validated Ensemble Models for small-sample DOE and chemometric applications, with (relaxed) elastic-net base learners for Gaussian and binomial responses built on **glmnet** using validation-weighted information-criterion analogs. Together with the permutation whole-model test and the random-search desirability scoring and candidate-selection tools, **SVEMnet** offers an end-to-end workflow for mixture-constrained multi-response optimization in a single toolchain. The software is aimed at practitioners running small-sample (*e.g.*, tens of runs) chemometric, pharmaceutical, and industrial DOE studies for formulation optimization, often involving mixture factors alongside numeric and categorical process factors.

SVEMnet is designed for single-error-stratum settings in which runs can be treated as independent resampling units. Hierarchical split-plot and other multi-stratum designs with random effects are not supported by **SVEM** and would require substantial methodological changes beyond the scope of this

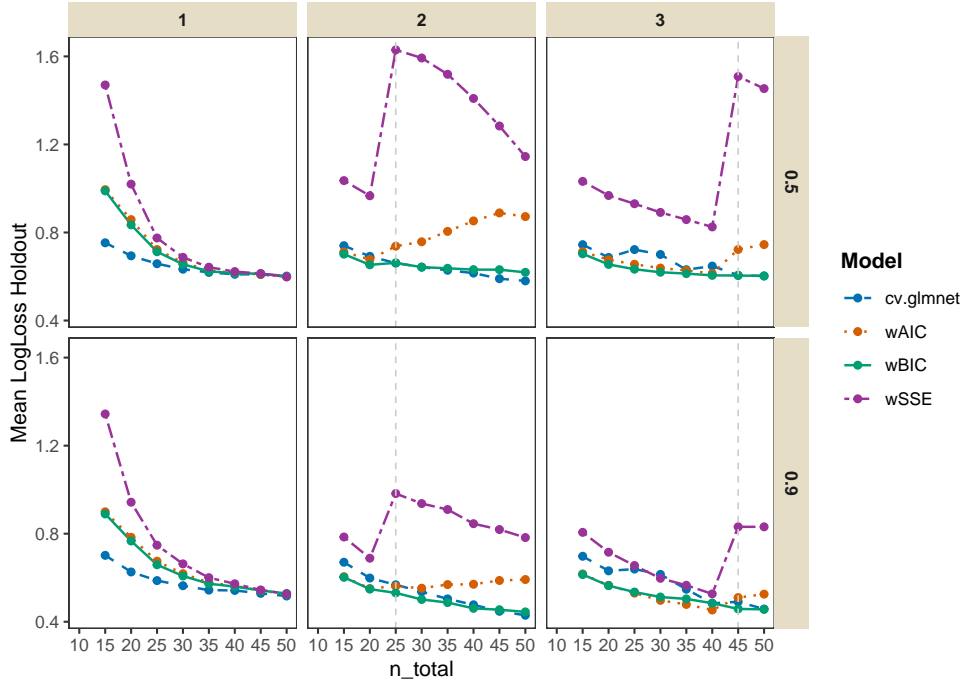


Figure 6: Binomial simulations: mean holdout log-loss versus n_{total} by target R^2 (rows) and fitted expansion order (columns). Vertical lines mark interpolation boundaries $n_{\text{total}} = p_{\text{full}}$.

paper. In addition, the validation-weighted information-criterion analogs, WMT “ p -values,” and mean-in-specification probabilities are intended as heuristic tuning, ranking, and diagnostic summaries rather than as fully calibrated inferential quantities. We therefore recommend reporting key tuning budgets and performing simple sensitivity checks (e.g., varying seeds, bootstrap/permutation budgets, desirability parameters, or expansion order) when conclusions are marginal.

Appendix A. Validation-weighted criterion and guardrails

This appendix records the validation-weighted selection criteria used in *SVEMnet*.

Appendix A.1. Gaussian criterion

Within each FRW replicate, let λ index a point on the elastic-net path, let k_λ denote the number of nonzero coefficients (including the intercept), and let w_i^{valid} be the FRW validation weights, rescaled to have mean one so that $\sum_i w_i^{\text{valid}} = n$. Write $r_{\lambda,i} = y_i - \hat{y}_{\lambda,i}$ for the residual at observation i under λ , and define the weighted sum of squared errors

$$\text{SSE}_w(\lambda) = \sum_i w_i^{\text{valid}} r_{\lambda,i}^2. \quad (\text{A.1})$$

For Gaussian responses we consider three selectors: a loss-only rule based on $\text{SSE}_w(\lambda)$ and two information-criterion analogs. The loss-only selector **wSSE** minimizes $\text{SSE}_w(\lambda)$ over the path. The validation-weighted AIC and BIC analogs minimize

$$C_g(\lambda) = n \log \left(\frac{\text{SSE}_w(\lambda)}{n} \right) + g k_\lambda, \quad g \in \{2, \log(n_{\text{eff}}^{\text{adm}})\}, \quad (\text{A.2})$$

which yield, respectively, a validation-weighted AIC analog (\mathbf{wAIC} , $g = 2$) and a validation-weighted BIC analog (\mathbf{wBIC} , $g = \log(n_{\text{eff}}^{\text{adm}})$) [12, 13, 14]. In the unweighted case, $w_i^{\text{valid}} \equiv 1$ and $\text{SSE}_w(\lambda)$ reduces to the usual residual sum of squares $\text{RSS}(\lambda)$. In that case $C_g(\lambda)$ reduces to $n \log\{\text{RSS}(\lambda)/n\} + g k_\lambda$, which is the standard Gaussian AIC/BIC form (up to an additive constant independent of λ).

Following Kish [46], we summarize the variability of the validation weights via an effective sample size

$$n_{\text{eff}} = \frac{(\sum_i w_i^{\text{valid}})^2}{\sum_i (w_i^{\text{valid}})^2} \quad (\text{A.3})$$

and use the bounded quantity

$$n_{\text{eff}}^{\text{adm}} = \min\{n, \max(2, n_{\text{eff}})\} \quad (\text{A.4})$$

when forming the BIC-style penalty $\log(n_{\text{eff}}^{\text{adm}}) k_\lambda$. With mean-one FRW weights, $2 \leq n_{\text{eff}}^{\text{adm}} \leq n$.

For the information-criterion selectors (\mathbf{wAIC} , \mathbf{wBIC}) we additionally impose

$$k_\lambda - 1 < n_{\text{eff}}^{\text{adm}}, \quad (\text{A.5})$$

so that the number of non-intercept coefficients is strictly smaller than the effective number of validation observations. Path points violating this inequality are treated as inadmissible when evaluating $C_g(\lambda)$. This guardrail helps stabilize model selection near the interpolation boundary $n = p_{\text{full}}$ [47, 36, 16, 48].

Appendix A.2. Binomial (logistic) criterion

For binomial responses we minimize a deviance-style quantity plus a complexity penalty. Let $\ell_{\text{valid}}(\lambda)$ denote the weighted log-likelihood on the FRW validation copy under path point λ , and let $\text{NLL}(\lambda) = -\ell_{\text{valid}}(\lambda)$ be the corresponding weighted negative log-likelihood. The AIC- and BIC-style selectors minimize

$$C_g^{(\text{bin})}(\lambda) = -2\ell_{\text{valid}}(\lambda) + g k_\lambda = 2\text{NLL}(\lambda) + g k_\lambda, \quad g \in \{2, \log(n_{\text{eff}}^{\text{adm}})\}, \quad (\text{A.6})$$

which differs from the usual binomial deviance only by an additive constant independent of λ . In the implementation we work directly with $\text{NLL}(\lambda)$ and form $C_g^{(\text{bin})}(\lambda)$ as $2 \times \text{NLL} + g k_\lambda$ for these selectors. For \mathbf{wAIC} and \mathbf{wBIC} the same effective-size quantity $n_{\text{eff}}^{\text{adm}}$ and guardrail $k_\lambda - 1 < n_{\text{eff}}^{\text{adm}}$ are used as in the Gaussian case.

When $g = 0$ the selector is a loss-only rule based on the weighted negative log-likelihood; for consistency with the Gaussian setting we retain the label \mathbf{wSSE} for this case even though it is based on negative log-likelihood rather than squared error. Ensemble predictions are formed by averaging bootstrap-member-predicted probabilities on the response scale.

Appendix B. Supplementary robustness and diagnostic analyses

This appendix provides additional robustness checks and diagnostics. All simulation scripts are available in the Mendeley Data repository [44].

Appendix B.1. Focused interpolation-boundary sweep

To run an explicit check of boundary behavior near the interpolation point, we ran a fine sweep of the total run size n in a representative Gaussian setting, drawing a new true response surface and a new (noiseless) evaluation set in each replicate. The deterministic expansion order was fixed at Order 2, with $p_{\text{full}} = 25$ predictors (including main effects, two-way interactions, and quadratic terms). We varied n over $\{20, 21, \dots, 30\}$, spanning the interpolation boundary $n \approx p_{\text{full}}$, and used 150 replicates per n (new training designs and noise per replicate) with a target strength of $R^2 = 0.5$.

Figure B.7 shows the mean holdout log-NRMSE and the mean of the per-replicate median selected model size k_λ as a function of n . The loss-only selector **wSSE** exhibits a pronounced “peaking”/instability near the boundary (worst at $n = 24$ and $n = 25$), while **wAIC** and **wBIC** remain stable and avoid selecting near-saturated models. At the boundary $n = 25$, the mean holdout NRMSE under **wSSE** was 3.07, compared to 0.87 and 0.86 for **wAIC** and **wBIC**, respectively (repeated `cv.glmnet` baseline: 0.92). Consistent with the manuscript discussion, **wAIC**/**wBIC** act as validation-weighted tuning-score analogs under FRW rather than classical information criteria with formal asymptotic justification; empirically, they suppress boundary peaking by penalizing overly large effective model size within each FRW replicate.

Appendix B.2. Design robustness and effect-density/distribution robustness

To qualify the simulation evidence beyond the Latin-hypercube baseline and sparse-effect settings, we repeated a representative Gaussian simulation under two design regimes: (i) a Latin hypercube design (LHS; baseline in the paper) and (ii) a face-centered central composite design (CCD), matched to the same factor space. For computational simplicity in this robustness check, we restrict attention to the four continuous factors $X_1: X_4 \in [-1, 1]$ (no categorical factor), and we fit the same quadratic (Order 2) deterministic expansion used in the main Gaussian study.

The CCD uses the standard face-centered structure for $k = 4$ continuous factors: 2^4 factorial points plus $2k$ axial (face) points, augmented with two center points, for a total of $n_{\text{total}} = 2^4 + 2k + 2 = 24 + 2 = 26$ runs. The LHS design is generated on the same $[-1, 1]^4$ domain with $n_{\text{total}} = 26$ runs.

To study sparsity sensitivity, we used three coefficient settings for the true surface: a sparse Laplace regime (baseline), a sparse Gaussian regime, and a denser Gaussian regime, each evaluated at two target signal strengths ($R^2 \in 0.5, 0.9$). Each design-effect- R^2 setting used 500 independent replicates (new coefficient vector, training data, and noise per replicate; the LHS design is regenerated each replicate, while the CCD uses the fixed face-centered point set with randomized run order), and all methods were scored on a large noiseless holdout set.

Figure B.8 summarizes mean holdout log-NRMSE (with 95% Monte Carlo standard-error intervals). In this study the CCD yields uniformly lower error than the matched LHS design across all settings and methods, which is expected because the data-generating surface is quadratic and therefore closely aligned with the model class that CCDs are designed to estimate efficiently. Within this (best-case) CCD regime, **wAIC** and **wBIC** remain competitive with repeated `cv.glmnet`; however, for the CCD with a dense-Normal coefficient regime, repeated CV is better, most clearly at high signal ($R^2 = 0.9$), and only very slightly at $R^2 = 0.5$.

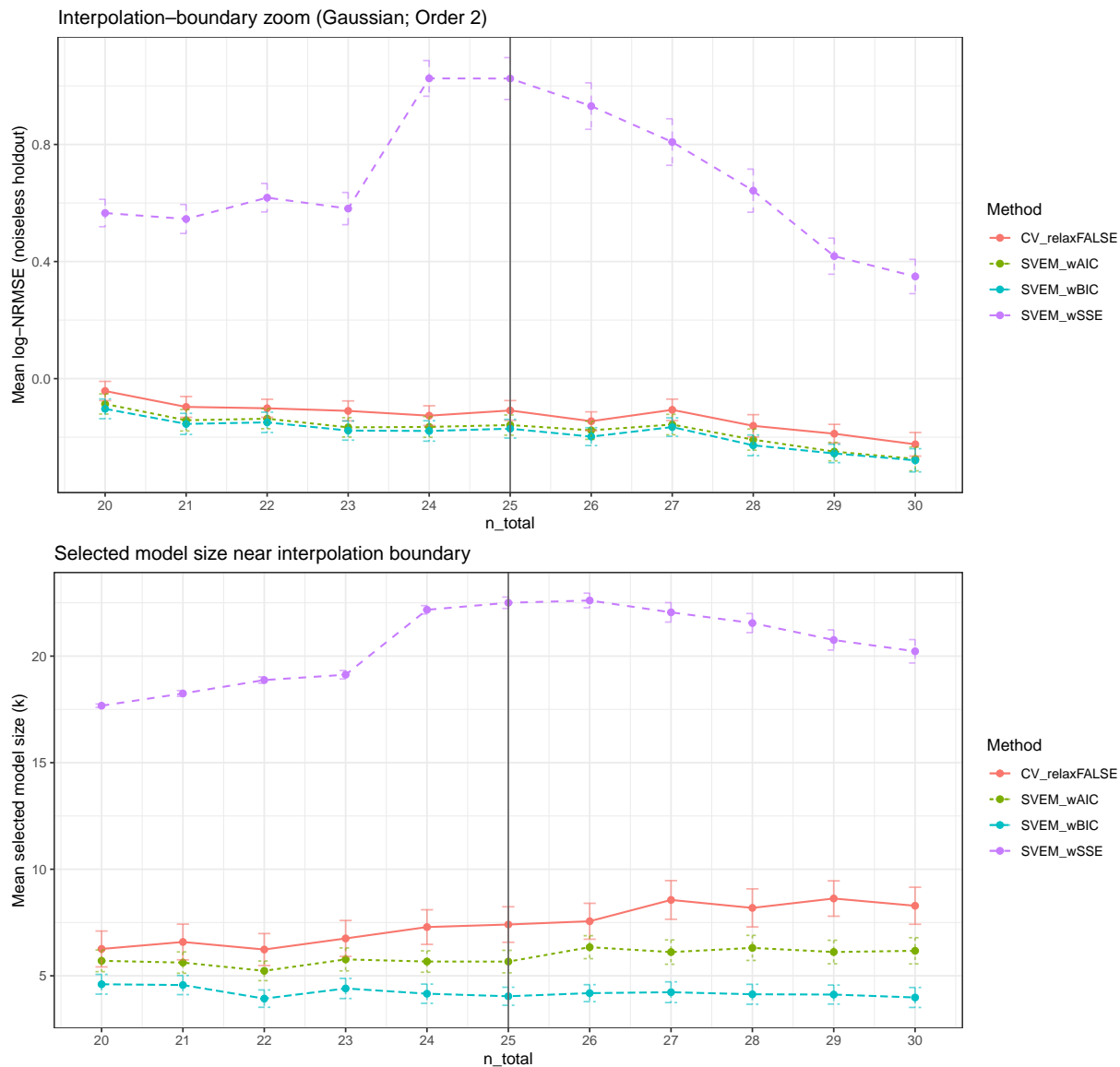


Figure B.7: Focused interpolation-boundary sweep (Gaussian). Top: mean holdout log-NRMSE versus n near $p_{\text{full}} = 25$. Bottom: mean k_{λ} (per-replicate k_{λ} medians over SVEM bootstraps) versus n .

More broadly, these results should be interpreted as complementary to (not a replacement for) the paper’s baseline space-filling evidence: in formulation optimization one often fits a large expansion with many candidate interactions and polynomial terms to hedge against surface complexity, while expecting that only a small subset of terms is active (the sparsity-of-effects principle). Highly structured classical designs can perform extremely well when the assumed model class is correct, but when the active terms are not well supported by the design (or when the working expansion is misspecified relative to the true surface), the resulting model can be biased and predictive performance can degrade [20]. A systematic study of design choice under misspecification and varying sparsity—and how SVEMnet and repeated CV behave in those regimes—is a natural direction for future work, and the released SVEMnet package and shared simulation code make such extensions straightforward to implement.

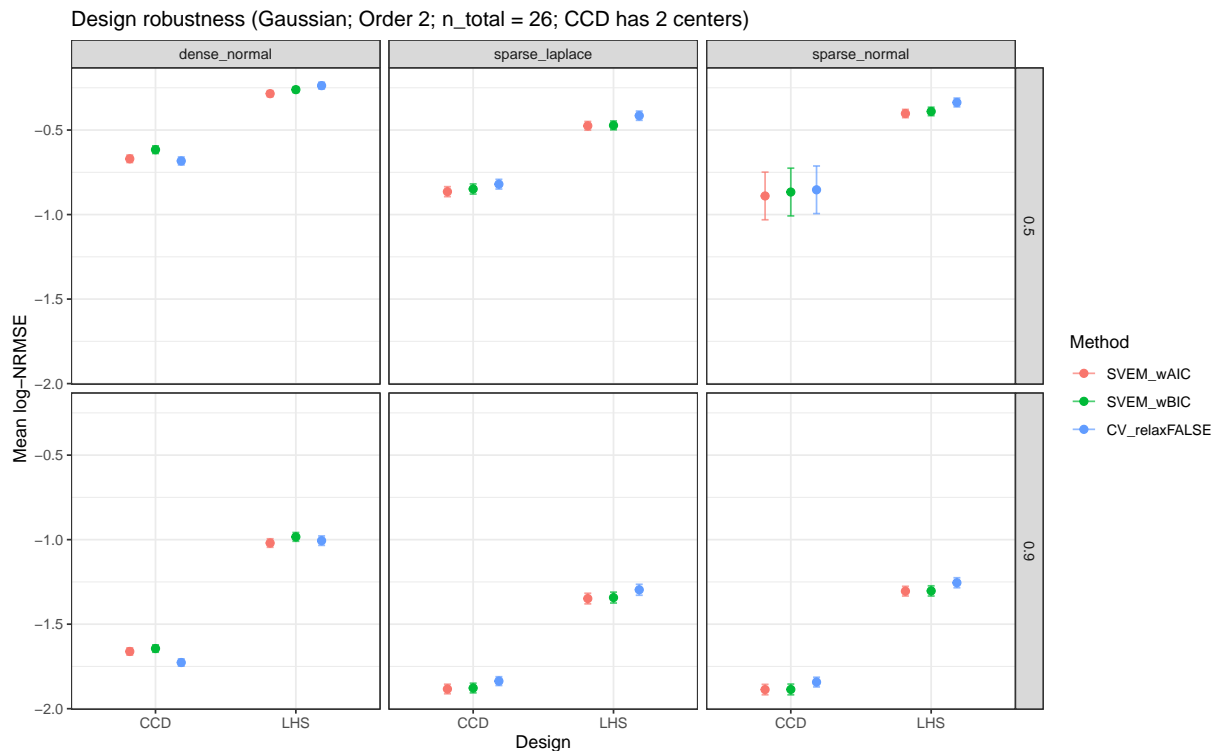


Figure B.8: Design robustness and effect-density/distribution robustness (Gaussian; continuous factors $X_1:X_4$ only; $n_{\text{total}} = 26$; Order 2). Mean holdout log-NRMSE (95and two target signal levels ($R^2 \in \{0.5, 0.9\}$)). The CCD uses the standard face-centered $k = 4$ structure ($2^4 + 2k$) with two center points.

Appendix B.3. Relaxation diagnostics

Gaussian. To make the bias–variance and relaxation behavior explicit, we ran a representative Gaussian diagnostic with a fixed true surface (sparse-Laplace coefficients) and a fixed noiseless holdout set. We re-sampled the training design and noise across $N_{\text{rep}} = 500$ replicates using an Order 2 expansion with $n_{\text{total}} = 30$ and target $R^2 = 0.9$. We compared four methods: (i) wAIC with relaxation enabled, (ii) wAIC with relaxation disabled, (iii) a repeated `cv.glmnet` baseline with relaxation disabled, and (iv) a repeated `cv.glmnet` baseline with relaxation enabled. To reduce tuning variability in this diagnostic and to keep λ comparisons interpretable, all fits use a lasso-only grid ($\alpha = 1$).

For each method, we recorded holdout NRMSE/log-NRMSE and a prediction-scale decomposition of holdout mean-squared error into Bias² and Var components, defined as $\text{Bias}^2 = \mathbb{E}_x\{(\mathbb{E}_r \hat{y}_r(x) - y(x))^2\}$ and $\text{Var} = \mathbb{E}_x\{\text{Var}_r(\hat{y}_r(x))\}$, where r indexes training replicates and expectations average over holdout points. We additionally recorded, per replicate, the selected regularization level λ (for `SVEMnet`, summarized as the median of $\log_{10}(\lambda)$ across bootstrap-selected path points; for repeated CV, the single selected $\log_{10}(\lambda)$).

Figure B.9 shows the resulting bias–variance decomposition and the distribution of selected $\log_{10}(\lambda)$ across replicates. In this setting, relaxation exhibits the expected trade-off: it lowers bias but increases variance. For wAIC, relaxation reduces Bias² (1.10 vs 1.51) while increasing Var (1.25 vs 0.99), yielding a small improvement in overall MSE (2.35 vs 2.50) and mean holdout NRMSE (0.439 vs 0.454). For repeated CV, relaxation similarly lowers bias (0.93 vs 1.35) but increases variance more sharply (2.52 vs 1.68), worsening overall MSE (3.45 vs 3.03) and mean NRMSE (0.528 vs 0.499). In the relaxed `SVEMnet` fits, the

Table B.3: WMT stability check for the LNP example. For each response and permutation budget (n_{perm}), values shown are median [min, max] across five random seeds.

Response	n_{perm}	p (median [min,max])	multiplier (median [min,max])
Size	150	$1e-16$ [$1e-16$, $1e-16$]	16 [16, 16]
Potency	150	$1e-16$ [$1e-16$, $4.45e-7$]	16 [6.35, 16]
PDI	150	0.832 [0.765, 0.935]	0.08 [0.029, 0.12]
Size	500	$1e-16$ [$1e-16$, $1e-16$]	16 [16, 16]
Potency	500	$2.23e-11$ [$5.42e-13$, $6.86e-8$]	10.7 [7.16, 12.3]
PDI	500	0.833 [0.783, 0.9]	0.079 [0.046, 0.11]

strongest relaxation available on the fixed grid was selected throughout ($\gamma = 0.2$), so we omit a separate γ plot and focus on the induced changes in prediction error and the λ distribution. To keep the relaxed search computationally tractable, **SVEMnet** evaluates a coarse fixed grid $\gamma \in \{0.2, 0.6, 1.0\}$ within each bootstrap replicate, where $\gamma = 1$ corresponds to the standard (non-relaxed) elastic-net fit at the selected λ , and smaller γ values apply a less-shrunk refit on the same active set (with the limiting case $\gamma \rightarrow 0$ approaching an unpenalized refit on the selected active predictors).

Binomial. We repeated an analogous diagnostic under a representative binomial setting ($n = 25$, Order 2, target $R^2 = 0.5$, $N_{\text{rep}} = 200$), comparing **wBIC** and repeated **cv.glmnet** with relaxation enabled/disabled. The binomial case reinforces the recommendation in the main text to disable relaxation: in this run, relaxation increased prediction variance and worsened holdout log-loss for both selectors. Mean log-loss was 0.345 for non-relaxed **wBIC** and 0.347 for non-relaxed repeated CV, versus 0.371 and 0.362 for the relaxed versions.

Appendix B.4. LNP example: WMT stability over random seeds and permutation budgets

Because WMT is a Monte Carlo diagnostic, we performed a small stability check for the LNP example by repeating `svem_wmt_multi()` under five random seeds and two permutation budgets ($n_{\text{perm}} = 150$ (default) and $n_{\text{perm}} = 500$), holding all other settings fixed (shared deterministic expansion and mixture constraints). Table B.3 summarizes the approximate whole-model p -values and the corresponding WMT multipliers.

These p -values are produced by the same parametric-tail procedure used in the package: WMT fits a flexible SHASH distribution to the permutation distance distribution and then reports the fitted right-tail probability for the observed distance. Because this is an extrapolated tail estimate rather than the raw empirical permutation fraction, values can be much smaller than $1/(n_{\text{perm}} + 1)$; we therefore interpret them as approximate diagnostic probabilities rather than exact permutation-test p -values.

Across seeds and budgets, Size and Potency consistently show strong global signal (always $p \leq 4.45 \times 10^{-7}$, often at the numerical floor), whereas PDI remains weak (here p in the range 0.76–0.94). Increasing n_{perm} narrows the Potency p -values but does not change the qualitative conclusion.

Appendix B.5. LNP example: desirability calibration sensitivity

To operationalize desirability calibration and provide a lightweight sensitivity check, we held the fitted SVEM surrogate models fixed and re-scored random-search LNP candidates under several small, practitioner-relevant perturbations of the desirability mapping. We repeated this across five independent

Table B.4: Desirability sensitivity (LNP example), $K = 50$. Top- K overlap vs. the default desirability mapping under small perturbations. Entries are median [min,max] over five independent random candidate draws ($N = 25,000$ each). Overlap reports $|A \cap B|$ out of K .

Variant	Description (brief)	$ A \cap B $	Jaccard
V1_uniform_shape2_sanity	Uniform DS shape = 2 (sanity check)	50 [50,50]	1.000 [1.000,1.000]
V2_weights_pot_mild	Mild reweight toward potency (0.65/0.25/0.10)	47 [46,48]	0.887 [0.852,0.923]
V3_size_shape125	Size desirability shape = 1.25 (mildly steeper)	46 [42,48]	0.852 [0.724,0.923]
V4_bounds_tighten5	Tighten inferred acceptables by 5% of span	50 [50,50]	1.000 [1.000,1.000]
V6_spec_bounds_alt	Spec-anchored acceptable bounds (alternative)	32 [28,37]	0.471 [0.389,0.587]

Table B.5: Desirability sensitivity (LNP example), $K = 200$. Top- K overlap vs. the default desirability mapping under small perturbations. Entries are median [min,max] over five independent random candidate draws ($N = 25,000$ each). Overlap reports $|A \cap B|$ out of K .

Variant	Description (brief)	$ A \cap B $	Jaccard
V1_uniform_shape2_sanity	Uniform DS shape = 2 (sanity check)	200 [200,200]	1.000 [1.000,1.000]
V2_weights_pot_mild	Mild reweight toward potency (0.65/0.25/0.10)	187 [185,188]	0.878 [0.860,0.887]
V3_size_shape125	Size desirability shape = 1.25 (mildly steeper)	191 [186,193]	0.914 [0.869,0.932]
V4_bounds_tighten5	Tighten inferred acceptables by 5% of span	200 [199,200]	1.000 [0.990,1.000]
V6_spec_bounds_alt	Spec-anchored acceptable bounds (alternative)	168 [159,168]	0.724 [0.660,0.724]

random candidate draws ($N = 25,000$ candidates per draw, with the same mixture constraints) and, within each draw, compared the resulting top- K candidate sets against the default mapping using Jaccard overlap. We report results for $K \in \{50, 200\}$, where $K = 200$ provides a broad stability summary and $K = 50$ reflects a more stringent “top list”.

In this sensitivity exercise, “acceptable bounds” refer to the per-response Derringer–Suich mapping parameters that define the onset of full desirability (e.g., a lower acceptable value for a “maximize” goal, or an upper acceptable value for a “minimize” goal). Under the default mapping, these acceptable bounds are inferred automatically from the predicted response distributions over the candidate set within each draw (using a quantile-anchored range with a small span floor for stability; see code in the Mendeley repository [44] for details). Variant `V4_bounds_tighten5` then tightens these inferred acceptable bounds by 5% of the inferred span (within the same draw), representing a mild perturbation around the default anchoring. In contrast, `V6_spec_bounds_alt` replaces the inferred acceptable bounds with fixed, practitioner-chosen “specification-anchored” ranges (Potency: 78–95; Size: 50–100; PDI: 0.10–0.25), while keeping the same goals and weights; this isolates sensitivity to how acceptable ranges are anchored rather than to small local perturbations around a fixed anchoring.

Tables B.4–B.5 show that mild perturbations to objective weights, a single-response shape exponent, or modest tightening of the inferred acceptable bounds yield high stability of the top set. Uniformly scaling all shape exponents leaves the top- K set unchanged. In contrast, the specification-anchored calibration produces a partially different top set, consistent with recommendations being more sensitive to how practitioners anchor acceptable ranges than to modest curvature/weight perturbations around a fixed anchoring.

Appendix B.6. LNP example: candidate stability under adjacent expansion orders

To demonstrate stability of candidate sets under adjacent expansion-order choices, we fit two adjacent deterministic expansions (Orders 2 and 3) to the same LNP training data and compared the top- K candidate sets ($K = 200$) under the primary score. The overlap was 155/200 candidates (Jaccard = 0.633), indicating moderate stability: many top candidates persist across orders, but some candidates shift ranking when the expansion is changed. In practice, this motivates the lightweight order-sensitivity check recommended in the main text.

Appendix C. Supplementary multiple-comparison tables

For completeness we provide Tukey–Kramer multiple-comparison summaries for the Gaussian and binomial simulations. These tables correspond to the mixed-model analyses described in Section 4, based on 250 (Gaussian) and 200 (binomial) independent simulation replicates for each combination of n_{total} , **Target_R2**, and **Setting** at the quadratic expansion (Order 2); full CSV outputs are included in the replication bundle [44].

For all Tukey–Kramer analyses we fixed the expansion at the correctly specified quadratic order (Order 2) and fit linear mixed models in JMP Pro 19 with **Setting** as the primary factor of interest, n_{total} , **Target_R2**, and their interaction as categorical fixed effects, and simulation run ID as a random intercept. Pairwise differences between settings were assessed using Tukey–Kramer honestly significant difference comparisons of the model-based least-squares means, controlling the familywise error rate at $\alpha = 0.05$. Settings that do not share a letter differ significantly, and smaller least-squares means correspond to better performance (lower log-NRMSE or log-loss). Here **relaxTRUE/FALSE** indicates whether relaxed base learners are used, **lasso/default** indicates the pure lasso case ($\alpha = 1$) versus the mixed- α grid $\alpha \in \{0.5, 1\}$, and in Table C.6 the suffix **dbTRUE/FALSE** indicates whether the post-hoc debiasing step is applied. In Table C.7 all configurations use **dbFALSE**.

To avoid inflating the number of pairwise comparisons with a clearly noncompetitive method, the loss-only **wSSE** selector was omitted from the Tukey–Kramer analyses. The overview plots in Figures 4 and 6 show **wSSE** performing uniformly poorly across the simulation grid.

Table C.6: Tukey–Kramer HSD connecting letters for the Gaussian simulation (response: log-NRMSE on a noiseless holdout; smaller least-squares means are better; rows are sorted from worst to best).

Setting	Least-squares mean	Group
CV_relaxTRUE_lasso_dbTRUE	-0.4550838	A
CV_relaxTRUE_default_dbTRUE	-0.4568168	A
CV_relaxTRUE_lasso_dbFALSE	-0.4784299	B
CV_relaxTRUE_default_dbFALSE	-0.4795369	B
SVEM_wBIC_relaxFALSE_lasso_dbFALSE	-0.4872574	BC
SVEM_wBIC_relaxFALSE_default_dbFALSE	-0.4873671	BC

Setting	Least-squares mean	Group
CV_relaxFALSE_lasso_dbTRUE	-0.4890622	C
CV_relaxFALSE_default_dbTRUE	-0.4955437	C
CV_relaxFALSE_lasso_dbFALSE	-0.5125708	D
SVEM_wBIC_relaxFALSE_default_dbTRUE	-0.5153720	DE
SVEM_wBIC_relaxFALSE_lasso_dbTRUE	-0.5154061	DE
SVEM_wAIC_relaxFALSE_lasso_dbTRUE	-0.5173612	DE
SVEM_wAIC_relaxFALSE_default_dbTRUE	-0.5173877	DE
CV_relaxFALSE_default_dbFALSE	-0.5182228	DE
SVEM_wBIC_relaxTRUE_lasso_dbTRUE	-0.5202504	DE
SVEM_wBIC_relaxTRUE_default_dbTRUE	-0.5205100	DE
SVEM_wAIC_relaxTRUE_default_dbTRUE	-0.5240749	E
SVEM_wAIC_relaxTRUE_lasso_dbTRUE	-0.5243519	E
SVEM_wAIC_relaxFALSE_default_dbFALSE	-0.5429558	F
SVEM_wAIC_relaxFALSE_lasso_dbFALSE	-0.5436361	F
SVEM_wBIC_relaxTRUE_lasso_dbFALSE	-0.5495013	F
SVEM_wBIC_relaxTRUE_default_dbFALSE	-0.5501097	F
SVEM_wAIC_relaxTRUE_default_dbFALSE	-0.5745804	G
SVEM_wAIC_relaxTRUE_lasso_dbFALSE	-0.5746790	G

Table C.7: Tukey–Kramer HSD connecting letters for the binomial simulation (response: `LogLoss_Holdout`; smaller least-squares means are better; rows are sorted from worst to best).

Setting	Least-squares mean	Group
CV_relaxTRUE_default	0.938427	A
CV_relaxTRUE_lasso	0.896920	A
SVEM_wAIC_relaxTRUE_default	0.808413	B
SVEM_wAIC_relaxTRUE_lasso	0.800409	B
SVEM_wBIC_relaxTRUE_default	0.735577	C
SVEM_wBIC_relaxTRUE_lasso	0.724202	C
SVEM_wAIC_relaxFALSE_default	0.683151	D
SVEM_wAIC_relaxFALSE_lasso	0.683002	D
CV_relaxFALSE_lasso	0.602811	E
CV_relaxFALSE_default	0.593384	E
SVEM_wBIC_relaxFALSE_default	0.575261	E
SVEM_wBIC_relaxFALSE_lasso	0.575050	E

CRedit authorship contribution statement

Andrew T. Karl: Software; Writing - original draft.

Funding

This research did not receive any specific grant from funding agencies in the public, commercial, or not-for-profit sectors.

Declaration of competing interest

The author developed the **SVEMnet** package and the related JMP add-in. The author has no other competing financial interests or personal relationships that could have appeared to influence the work reported in this paper.

Declaration of generative AI and AI-assisted technologies in the manuscript and software preparation process

During the preparation of this manuscript and the accompanying software, the author used OpenAI GPT models as assistive tools. Under the author's direction, these models were used (i) to revise and proofread prose and (ii) to help draft the **SVEMnet** (and simulation) R code and associated documentation. All AI-generated text and code were reviewed, edited, and validated by the author before inclusion. All algorithmic design choices, statistical methodology, simulation design, and final implementation decisions were made by the author, who takes full responsibility for the content of the manuscript, the software, and all reported results.

Data and software availability

Data and replication. The R scripts, configuration files, and CSV outputs required to reproduce the simulations, figures, and LNP case study are available in the Mendeley Data repository [44].

Software. **SVEMnet** is available on CRAN: <https://doi.org/10.32614/CRAN.package.SVEMnet>. The analyses in this paper were run with **SVEMnet** v3.2.0; the corresponding source tarball is included in the replication archive [44]. Documentation includes a reference manual shipped with the package. The package was developed and tested under R 4.5.2 and licensed under GPL-2 | GPL-3.

JMP add-in. An optional JMP add-in, "Relaxed Elastic Net and Lasso SVEM using R" (<https://marketplace.jmp.com/appdetails/Relaxed+Elastic+Net+and+Lasso+SVEM+using+R>), is available via the JMP Marketplace. The add-in lets JMP users call **SVEMnet** for a saved `Fit Model` table script with Gaussian responses and obtain prediction and standard error formula columns.

Independently tested by

Daniel Fortune, Hexion, Inc., Katy, Texas, USA, installed `SVEMnet` (version 3.2.0) from a local build in R 4.5.2 and ran the supplemental `LNP_example_SVEMnet.R` code shown in Section 3 (and available for download from the repository [44]). The p -values printed to the console match those reported in Section 3. The CSV file of candidates saved successfully and contained the same entries (where `candidate_type` is equal to `best`) as shown in Table 1 and Table 2.

Acknowledgements

The author thanks Daniel Fortune for verifying installation and the core workflow, and the anonymous reviewers who provided feedback that led to improvements in the paper.

References

- [1] L. Breiman, Bagging predictors, *Machine learning* 24 (1996) 123–140.
- [2] T. Lemkus, C. Gotwalt, P. Ramsey, M. L. Weese, Self-validated ensemble models for design of experiments, *Chemometrics and Intelligent Laboratory Systems* 219 (2021) 104439. doi:10.1016/j.chemolab.2021.104439.
- [3] L. Xu, C. Gotwalt, Y. Hong, C. B. King, W. Q. Meeker, Applications of the fractional-random-weight bootstrap, *The American Statistician* 74 (2020) 345–358. doi:10.1080/00031305.2020.1731599.
- [4] C. Gotwalt, P. Ramsey, Model validation strategies for designed experiments using bootstrapping techniques with applications to biopharmaceuticals (2018).
- [5] A. T. Karl, A randomized permutation whole-model test heuristic for Self-Validated Ensemble Models (SVEM), *Chemometrics and Intelligent Laboratory Systems* 249 (2024) 105122. doi:10.1016/j.chemolab.2024.105122.
- [6] P. Ramsey, M. Gaudard, W. Levin, Accelerating innovation with space filling mixture designs, neural networks and svem, in: *JMP Discovery Conference, 2021*. URL: <https://community.jmp.com/t5/Abstracts/Accelerating-Innovation-with-Space-Filling-Mixture-Designs/ev-p/756841>, abstract and slides available from the JMP User Community.
- [7] G. Shmueli, To explain or to predict?, *Statistical Science* 25 (2010) 289–310. doi:10.1214/10-STS330.
- [8] H. Zou, T. Hastie, Regularization and variable selection via the elastic net, *Journal of the Royal Statistical Society Series B: Statistical Methodology* 67 (2005) 301–320.
- [9] J. H. Friedman, T. Hastie, R. Tibshirani, Regularization paths for generalized linear models via coordinate descent, *Journal of Statistical Software* 33 (2010) 1–22. doi:10.18637/jss.v033.i01.
- [10] N. Meinshausen, Relaxed lasso, *Computational Statistics & Data Analysis* 52 (2007) 374–393. doi:10.1016/j.csda.2006.12.019.

- [11] J. Friedman, T. Hastie, R. Tibshirani, The relaxed lasso, <https://glmnet.stanford.edu/articles/relax.html>, 2025. Article vignette.
- [12] H. Akaike, A new look at the statistical model identification, *IEEE Transactions on Automatic Control* 19 (1974) 716–723. doi:10.1109/TAC.1974.1100705.
- [13] G. Schwarz, Estimating the dimension of a model, *The Annals of Statistics* 6 (1978) 461–464. doi:10.1214/aos/1176344136.
- [14] K. P. Burnham, D. R. Anderson, *Model Selection and Multimodel Inference: A Practical Information-Theoretic Approach*, 2 ed., Springer, New York, 2002.
- [15] S. Raudys, R. P. Duin, Expected classification error of the fisher linear classifier with pseudo-inverse covariance matrix, *Pattern Recognition Letters* 19 (1998) 385–392. URL: <https://www.sciencedirect.com/science/article/pii/S0167865598000166>. doi:[https://doi.org/10.1016/S0167-8655\(98\)00016-6](https://doi.org/10.1016/S0167-8655(98)00016-6).
- [16] N. Krämer, On the peaking phenomenon of the lasso in model selection, *arXiv preprint* (2009). URL: <https://arxiv.org/abs/0904.4416>. doi:10.48550/arXiv.0904.4416. arXiv:0904.4416.
- [17] T. Hastie, A. Montanari, S. Rosset, R. J. Tibshirani, Surprises in high-dimensional ridgeless least squares interpolation, *Annals of Statistics* 50 (2022) 949–986. doi:10.1214/21-AOS2133.
- [18] R. Christensen, Linear model estimation and prediction for $p > n$, *The American Statistician* (2025) 1–9. doi:10.1080/00031305.2025.2566251, published online Nov. 11, 2025.
- [19] A. T. Karl, S. Essex, J. Wisnowski, H. Rushing, A workflow for lipid nanoparticle (LNP) formulation optimization using designed mixture–process experiments and Self-Validated Ensemble Models (SVEM), *Journal of Visualized Experiments* (2023) e65200. doi:10.3791/65200.
- [20] A. T. Karl, J. Wisnowski, H. Rushing, JMP Pro 17 remedies for practical struggles with mixture experiments, in: *JMP Discovery Conference*, 2022. doi:10.13140/RG.2.2.34598.40003/1, conference presentation.
- [21] P. Ramsey, C. Gotwalt, Model validation strategies for designed experiments using bootstrapping techniques with applications to biopharmaceuticals, in: *JMP Discovery Conference – Europe*, 2018. URL: https://community.jmp.com/t5/Abstracts/Model-Validation-Strategies-for-Designed-Experiments-Using/ev-p/849647/redirect_from_archived_page/true, abstract and slides available from the JMP User Community.
- [22] P. Ramsey, W. Levin, T. Lemkus, C. Gotwalt, Svem: A paradigm shift in design and analysis of experiments, in: *JMP Discovery Conference – Europe*, 2021. URL: <https://community.jmp.com/t5/Abstracts/SVEM-A-Paradigm-Shift-in-Design-and-Analysis-of-Experiments-2021/ev-p/756634>, abstract and slides available from the JMP User Community.
- [23] P. Ramsey, P. McNeill, Cmc, svem, neural networks, doe, and complexity: It’s all about prediction, in: *JMP Discovery Conference*, 2023. Conference presentation.

- [24] D. Mirzaiyanrajeh, E. V. Dave, J. E. Sias, P. Ramsey, Developing a prediction model for low-temperature fracture energy of asphalt mixtures using machine learning approach, *International Journal of Pavement Engineering* 24 (2023) 2024185. doi:10.1080/10298436.2021.2024185.
- [25] M. A. Korany, R. M. Youssef, M. A. A. Ragab, M. A. Afify, A synergistic chemometric combination for whiteness and greenness assessed hplc-dad assay of aqueous extracts of ivy and thyme and potassium sorbate in a syrup formula, *Microchemical Journal* 196 (2024) 109616. doi:10.1016/j.microc.2023.109616.
- [26] A. E. Mostafa, M. S. Eissa, A. Elsonbaty, K. Attala, R. A. Abdel Salam, G. M. Hadad, M. A. Abdelshakour, Computer-aided design of eco-friendly imprinted polymer decorated sensors augmented by self-validated ensemble modeling designs for the quantitation of drotaverine hydrochloride in dosage form and human plasma, *Journal of AOAC International* 106 (2023) 1361–1373. doi:10.1093/jaoacint/qsad049.
- [27] B. I. Hanafy, C.-E. Lu, K. Liu, A. Gallud, Prelive: A framework for predicting lipid nanoparticles in vivo efficacy and reducing reliance on animal testing, *Advanced Functional Materials* (2025) e25076. URL: <https://advanced.onlinelibrary.wiley.com/doi/abs/10.1002/adfm.202525076>. doi:<https://doi.org/10.1002/adfm.202525076>.
- [28] D. R. Jones, M. Schonlau, W. J. Welch, Efficient global optimization of expensive black-box functions, *Journal of Global Optimization* 13 (1998) 455–492.
- [29] B. Shahriari, K. Swersky, Z. Wang, R. P. Adams, N. de Freitas, Taking the human out of the loop: A review of Bayesian optimization, *Proceedings of the IEEE* 104 (2016) 148–175.
- [30] R. H. Myers, D. C. Montgomery, C. M. Anderson-Cook, *Response Surface Methodology: Process and Product Optimization Using Designed Experiments*, 4 ed., Wiley, 2016.
- [31] B. Jones, D. C. Montgomery, *Design of Experiments: A Modern Approach*, Wiley, Hoboken, NJ, 2020.
- [32] R. A. Lekivetz, B. A. Jones, Fast flexible space-filling designs with nominal factors for nonrectangular regions, *Quality and Reliability Engineering International* 35 (2019) 677–684. doi:10.1002/qre.2429.
- [33] B. Jones, D. M. Steinberg, Unrestricted bridge (U-Bridge) designs for settings with non-deterministic data, *Quality and Reliability Engineering International* 41 (2025) 3405–3414. doi:<https://doi.org/10.1002/qre.70050>.
- [34] M. D. McKay, R. J. Beckman, W. J. Conover, A comparison of three methods for selecting values of input variables in the analysis of output from a computer code, *Technometrics* 21 (1979) 239–245.
- [35] L. Lu, C. M. Anderson-Cook, Using sequential design of experiments and non-uniform space-filling designs for improved model selection, *Quality and Reliability Engineering International* 41 (2025) 3360–3372. doi:<https://doi.org/10.1002/qre.70039>.
- [36] T. Hastie, R. Tibshirani, J. Friedman, *The Elements of Statistical Learning: Data Mining, Inference, and Prediction*, 2nd ed., Springer, New York, 2009.

- [37] JMP, Overview of self-validated ensemble models, JMP Pro 19 Documentation, 2023. URL: <https://www.jmp.com/support/help/en/19.0/?os=win&source=application#page/jmp/overview-of-selfvalidated-ensemble-models.shtml>, section: Modeling.
- [38] H. Scheffé, Experiments with mixtures, *Journal of the Royal Statistical Society: Series B (Methodological)* 20 (1958) 344–360. doi:<https://doi.org/10.1111/j.2517-6161.1958.tb00299.x>.
- [39] M. C. Jones, A. Pewsey, Sinh-arcsinh distributions, *Biometrika* 96 (2009) 761–780. URL: <https://doi.org/10.1093/biomet/asp053>. doi:10.1093/biomet/asp053. arXiv:<https://academic.oup.com/biomet/article-pdf/96/4/761/588296/asp053.pdf>.
- [40] E. C. Harrington, The desirability function, *Industrial Quality Control* 21 (1965) 494–498.
- [41] G. Derringer, R. Suich, Simultaneous optimization of several response variables, *Journal of Quality Technology* 12 (1980) 214–219.
- [42] J. C. Gower, A general coefficient of similarity and some of its properties, *Biometrics* 27 (1971) 857–871.
- [43] L. Kaufman, P. J. Rousseeuw, *Finding Groups in Data: An Introduction to Cluster Analysis*, Wiley, New York, 1990.
- [44] A. Karl, Data and code for SVEMnet publication, 2025. URL: <https://doi.org/10.17632/2zshchrhjh.4>. doi:10.17632/2zshchrhjh.4.
- [45] J. A. Cornell, *Experiments with Mixtures: Designs, Models, and the Analysis of Mixture Data*, 3 ed., Wiley, 2002.
- [46] L. Kish, *Survey Sampling*, John Wiley & Sons, New York, 1965.
- [47] B. Efron, T. Hastie, I. Johnstone, R. Tibshirani, Least angle regression, *Annals of Statistics* 32 (2004) 407–499. doi:10.1214/009053604000000067.
- [48] M. Belkin, D. Hsu, S. Ma, S. Mandal, Reconciling modern machine-learning practice and the classical bias–variance trade-off, *Proceedings of the National Academy of Sciences* 116 (2019) 15849–15854. doi:10.1073/pnas.1903070116.

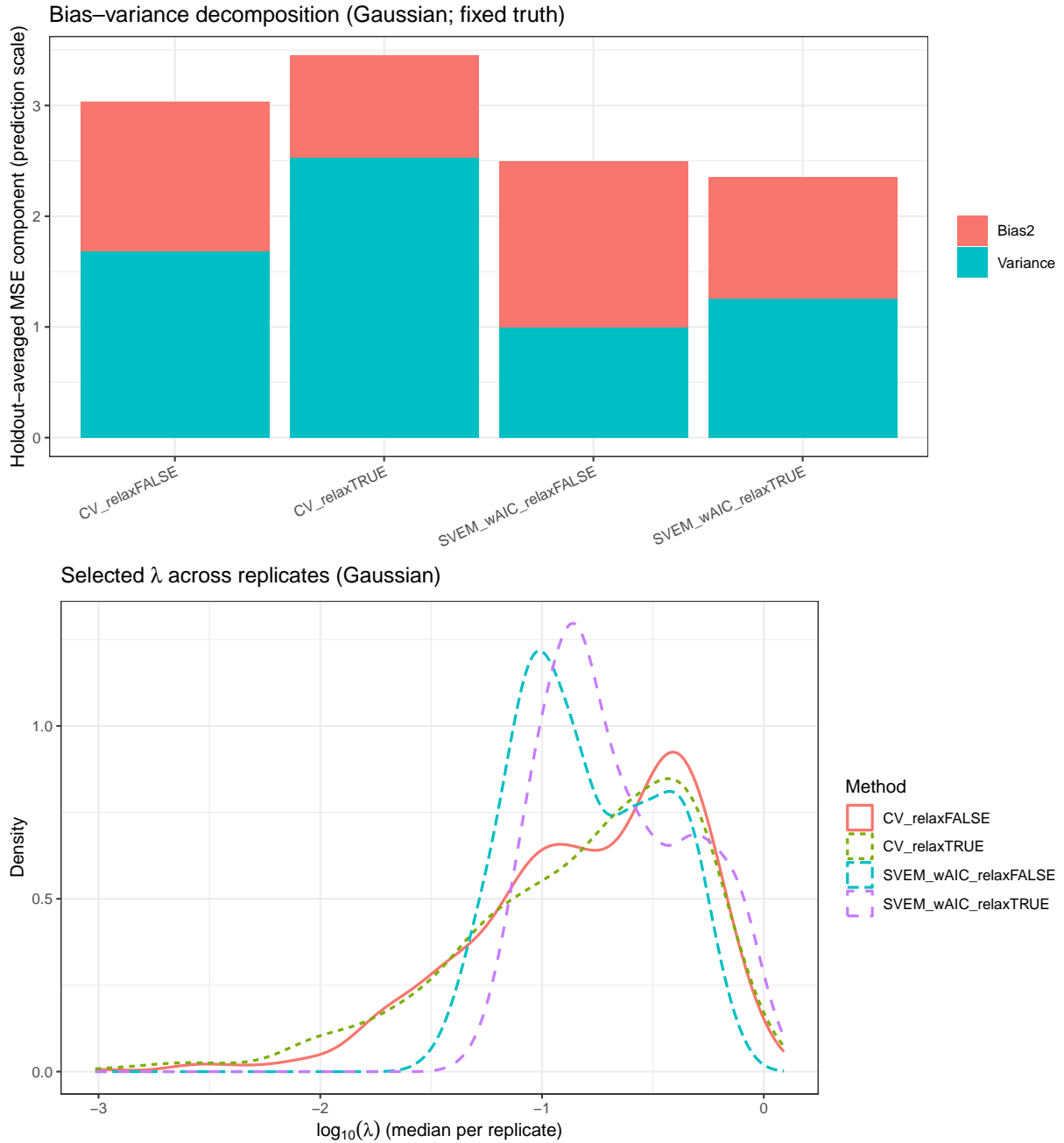


Figure B.9: Gaussian relaxation diagnostics ($n_{\text{total}} = 30$, Order 2, $N_{\text{rep}} = 500$, lasso-only $\alpha = 1$). Top: prediction-scale bias–variance decomposition on a fixed noiseless holdout set. Bottom: distribution of selected $\log_{10}(\lambda)$ across training replicates (per replicate: median across SVEM bootstraps; single selected value for repeated CV).